Journal of Banking & Finance 66 (2016) 19–34

Contents lists available at ScienceDirect

Journal of Banking & Finance

journal homepage: www.elsevier.com/locate/jbf

Pricing and hedging of derivatives in contagious markets

Thomas Kokholm *

Aarhus University, School of Business and Social Sciences, Department of Economics and Business Economics, Fuglesangs Allé 4, 8210 Aarhus V, Denmark

ARTICLE INFO

Article history:
Received 30 July 2014
Accepted 31 January 2016
Available online 9 February 2016

JEL classification:
G01
G13

Keywords:
Multivariate modeling
Contagion
Derivatives pricing
Jump processes
Hedging

ABSTRACT

It is well documented that stock markets are contagious. A negative shock to one market increases the probability of adverse shocks to other markets. We model this contagion effect by including mutually exciting jump processes in the dynamics of the indexes' log-returns. On top of this we add a stochastic volatility component to the dynamics. It is important to take the contagion effect into account if derivatives written on a basket of assets are to be priced or hedged. Due to the affine model specification the joint characteristic function of the log-returns is known analytically, and for two specifications we detail how the model can be calibrated efficiently to option prices. In total we calibrate over an extended period of time the specifications to options data on four US stock indexes, and show how the models achieve satisfactory pricing errors. We study the effect of contagion on multi-asset derivatives prices and show how for certain derivatives the impact is heavy. Moreover, we derive hedge ratios for European put and call options and perform a numerical experiment, which illustrates the impact of contagious jumps on option prices and hedge ratios. Mutually exciting processes have been analyzed for multivariate intensity modeling for the purpose of credit derivatives pricing, but have not been used for pricing/hedging options on equity indexes.

1. Introduction

It is well documented that stock markets are contagious. Markets are heavily interlinked, and losses spread across them. Moreover, financial contagion is magnified as fears of adverse market shocks tend to spread among investors, resulting in panic behavior. Hence, a negative shock to one market increases the probability of negative shocks to other markets, see Aït-Sahalia et al. (2015) and references therein for empirical documentation. We model this contagion effect by including mutually exciting jump processes in the dynamics of the indexes' log-returns, so that a jump in one market increases the intensities of more jumps in the same market and in other markets. Between jumps, the intensities revert to their long-run means. Clustering of jumps can also be achieved by for instance, letting the jump process be specified as a doubly stochastic Poisson process with stochastic intensity. However, this approach will not capture the direct feedback effect that jumps have on the probability of more jumps occurring. On top of this, we add a stochastic volatility component to the dynamics in order to introduce more flexibility in the return distribution. In a recent empirical study, Aït-Sahalia et al. (2015) show that a model of this type captures the observed joint evolution of equity index returns from different regions of the world.

Fig. 1 depicts an example of successive negative log-returns of the indexes Amex Biotechnology Index (BTK), the Morgan Stanley Technology index (MSH), the Securities Broker/Dealer index (XBD), and the Natural Gas index (XNG) over the period from Tuesday, November 4 to Monday, November 10, 2008. On Tuesday the XBD index and to a lesser degree the MSH index experienced a big drop in value, which was followed by additional drops in both indexes together with the XNG index on Wednesday. On Thursday all four indexes rebounced a bit with returns around 2%. Then on Friday the XBD index fell more than 8%, followed by significant decreases in all four indexes in the beginning of the next week. The model proposed in this paper is well-suited for modeling occurrences like this.

Multi-asset derivatives such as spread and correlation options are traded frequently over-the-counter and on exchanges, and it is important to take the contagion effect into account if they are to be priced or hedged (Fry-McKibbin et al., 2014). Structured products containing basket options are both traded on exchanges (Wallmeier and Diethelm, 2012) and also marketed to private investors (Jørgensen et al., 2011).

Multivariate jump and stochastic volatility models have been proposed in the academic literature, in e.g. Leoni and Schoutens (2008),

* Tel.: +45 87165216.
E-mail address: thko@econ.au.dk

http://dx.doi.org/10.1016/j.jbankfin.2016.01.012
0378-4266/

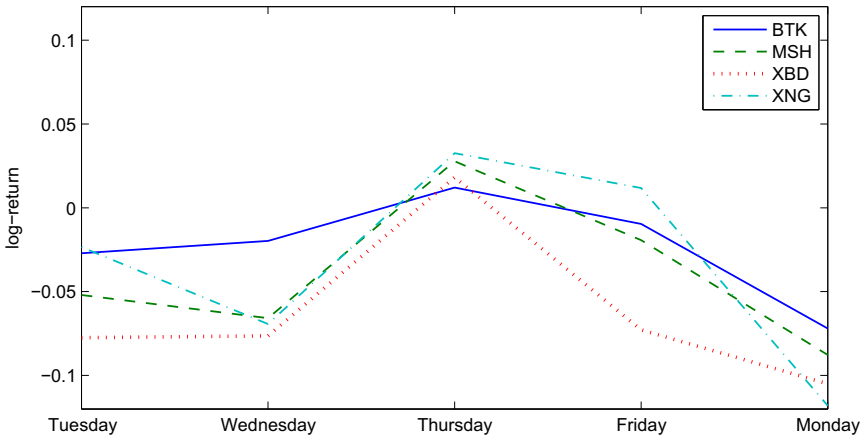

Fig. 1. Historical log-returns of the four indexes: BTK, MSH, XBD, and XNG over the week from November 4–10, 2008.

Gouriéroux et al. (2009), Luciano and Semeraro (2010), and Madan (2011) etc., but none of these are able to model contagious links between different indexes. Self-exciting jump processes were first introduced by Hawkes (1971) and have therefore also been given the name *Hawkes processes*. Hawkes processes have been applied in a number of different contexts, e.g. to model contagious diseases in epidemiology, earthquake occurrences, and in genome analysis etc. (see footNote 4 in Aït-Sahalia et al. (2015) for references). In a financial context, mutually exciting processes have been analyzed for multivariate intensity modeling for the purpose of credit modeling in Errais et al., 2010; Aıt-Sahalia et al., 2014, for optimal portfolio selection in Aït-Sahalia and Hurd (2015), and in market microstructure to model transaction times and price changes jointly at high frequency in Bowsher (2007), but have not been used for pricing/hedging options on equity indexes.

Due to the affine model specification, the joint characteristic function of the log-returns is known analytically (Duffie et al., 2000), and for two specifications we detail how the model can be calibrated efficiently to option prices using Fourier transform methods. In total, we calibrate the specifications to single name NASDAQ options data, across strikes and maturities, for the four sector indexes BTK, the MSH, the XBD, and the XNG and investigate their pricing performances over an extended period of time. Preferably, one should also add multi-asset derivatives to the calibration instruments, when calibrating a multivariate model, but due to lack of data we have not been able to do this. In order to reduce computational time, the calibration is performed in two steps. First, the parameters of the mutually exciting processes are calibrated for the indexes simultaneously to a subset of the options data. Second, the stochastic volatility dynamics are calibrated to the whole option surface on each index independently. In general, we find that the two considered multivariate contagion specifications are able to fit the four options markets comparable to the individually calibrated Heston dynamics in most of the maturity/strike spectra of the implied volatility surface.

Moreover, we study the impact of the contagion on the prices of multi-asset derivatives such as spread, correlation and basket options, and find it to have a heavy impact on correlation and basket option prices, while the spread option is less sensitive to the level of contagion.

Finally, we derive the model hedge ratios for European put and call options and study their historical performances in the hedging of European single-name options. Additionally, we perform a numerical study where we analyze the impact of the contagion on option prices and hedge ratios.

The rest of the paper is structured as follows: Section 2 defines an affine jump-diffusive process, introduces the model specifications and derives the characteristic function of the log-return processes. Furthermore, we consider two parametric examples. In Section 3 the two specifications are implemented on options data. Section 4 summarizes how knowledge of the characteristic function for the joint return process can be utilized for the pricing of spread and correlation options using Fourier transform methods, and the impact of the contagion parameters on multivariate option prices is studied. The hedging of European options are studied in Section 5 and finally Section 6 concludes.

2. Contagion modeling

Consider a filtered probability space $(\Omega, \mathcal{F}, \{\mathcal{F}_t\}_{t\geqslant 0}, \mathbb{Q})$, where $\{\mathcal{F}_t\}_{t\geqslant 0}$ is a right-continuous and complete filtration representing the history of the arbitrage-free markets. Assume that the m asset processes $S^1, \ldots, S^m$ are adapted to $\{\mathcal{F}_t\}_{t\geqslant 0}$ and that $\mathbb{Q}$ is a pricing measure. We will assume the instantaneous interest rate r_t and dividend yields q_t^is deterministic. We start this section by describing the general affine jump-diffusive setup before introducing the model specifications of the paper.

2.1. Affine jump-diffusions

Since the affine jump-diffusion model framework embeds all the models studied in this paper we start by detailing it here. A jump process is called affine if its arrival intensity is an affine function of an affine jump-diffusion with jump sizes drawn from a fixed distribution (see Duffie et al., 2000). A d-dimensioned Markovian process Y is an affine jump-diffusion if it solves

$$dY_t = \mu(Y_t, t)dt + \sigma(Y_t, t)dW_t + \sum_{i=1}^{m} \zeta^i d\underline{J}_t^i, \tag{1}$$

where W is a d-dimensional Wiener process and each $\underline{J}^i$ is a d-dimensional pure jump process whose component processes jump simultaneously with common intensity λ^i and fixed jump size distribution $\underline{F}^i$. For $i = 1, \ldots, m, \zeta^i \in \mathbb{R}^{d\times d}$ the coefficients have the form

$$\begin{aligned}
&\mu(y,t) = K_0(t) + K_1(t)y, \quad K_0(t) \in \mathbb{R}^d, \quad K_1(t) \in \mathbb{R}^{d\times d}\\
&\left(\sigma(y,t)\sigma(y,t)^\top\right)_{jk} = (H_0)_{jk}(t) + (H_1)_{jk}(t)\cdot y, \quad H_0(t) \in \mathbb{R}^{d\times d}, \quad H_1(t) \in \mathbb{R}^{d\times d\times d}\\
&\lambda^i(y,t) = \Lambda_0^i(t) + \Lambda_1^i(t)\cdot y, \quad \Lambda_0^i \in \mathbb{R}, \quad \Lambda_1^i(t) \in \mathbb{R}^d, \quad i = 1, \ldots, m,
\end{aligned}$$

where '·' denotes the scalar product. The reader is referred to Duffie et al. (2000) for technical conditions on the coefficients.

In all the cases we consider in this paper the coefficients are "well-behaved" and will not exhibit any time dependence. Hence, $K_0(t) = K_0, K_1(t) = K_1$ etc. Moreover, the jump-intensities will be strictly positive for all the jump specifications considered.

2.2. Mutually self-exciting asset dynamics

As contagion is introduced in the asset dynamics via multivariate Hawkes processes we start by giving a brief introduction of them here. The succeeding section introduces the asset dynamics.

2.2.1. Hawkes processes

Consider m increasing sequences of stopping times $\{\tau_n^i\}_{n\in\mathbb{N}_+}, i = 1,\dots,m$ and let the n'th jump in asset i at time τ_n^i be given by a random variable ϵ_n^i with probability distribution F^i, where all the jumps ϵ_n^i are independent across n and of all τ_n^i. From the sequences of stopping times and jumps we define $N_t^i = \sum_{n\geqslant 1} 1_{\{\tau_n^i \leqslant t\}}$ and $J_t^i = \sum_{n=1}^{N_t^i} \epsilon_n^i$. By modeling the intensities of jumps mutually self-exciting in the following two separate specifications with $\alpha_i, \bar{\lambda}_i > 0$ for all $i = 1,\dots,m$

$$d\lambda_t^i = \alpha_i\left(\bar{\lambda}_i - \lambda_t^i\right)dt + \sum_{j=1}^m \delta_{ij} dJ_t^j \tag{2}$$

$$d\lambda_t^i = \alpha_i\left(\bar{\lambda}_i - \lambda_t^i\right)dt + \sum_{j=1}^m \delta_{ij} dN_t^j, \tag{3}$$

we arrive at two separate multivariate Hawkes processes. When asset j jumps, the intensity λ^i of asset i increases and between jumps it decays exponentially with rate α_i towards $\bar{\lambda}_i$. The formulation (2) is used for multivariate default modeling in Errais et al. (2010) and allows the jump in the intensity λ^i to depend on the size dJ^j of the jump in asset j. This contrasts the second formulation (3) used in Aït-Sahalia et al. (2015) for equity modeling, where the intensity jumps when the assets jump, but with no sensitivity to the jump size.

For the concrete jump specifications applied in this paper one can verify that the model is well-specified in the sense that it is uniquely defined by the set of parameters which fulfills the admissibility conditions given in Kallsen (2006). The reader is referred to Appendix A for the details. For a more rigorous discussion of uniqueness and existence of affine processes the reader is referred to Duffie et al. (2003) and Kallsen (2006).

2.2.2. Asset dynamics

Let $S_t^i = S_0^i e^{\int_0^t (r_t - q_t^i)dt + X_t^i}$ and assume X_t^i has the dynamics

$$dX_t^i = \mu_t^i dt + \sqrt{V_t^i} dW_t^i + dJ_t^i \tag{4}$$

$$dV_t^i = \kappa_i\left(\overline{V}_i - V_t^i\right)dt + \eta_i\sqrt{V_t^i} dZ_t^i, \tag{5}$$

where W^i and Z^i are correlated Wiener processes with correlation coefficient ρ_i. We will assume the jump process J^i independent of the Wiener processes W^i and Z^i. The parameters in the Heston variance dynamics $\kappa_i, \overline{V}_i, \eta_i$ are positive constants. We note here that the tractability of the model is ensured for any tractable specification of the stochastic variance process V^i. The model dynamics (4) belongs to the class of affine jump-diffusions with the coefficients for the jump part of the process given explicitly in Section 2.3.2.

If in the first formulation (2) it holds that (Karabash, 2012)

$$\alpha_i > \sum_{j=1}^m \delta_{i,j} \int_{\mathbb{R}} y\, dF^j(y), \tag{6}$$

and in the second formulation (3) that

$$\alpha_i > \sum_{j=1}^m \delta_{i,j}. \tag{7}$$

then the long-run mean of the intensity in the two specifications are bounded and equal to

$$\lim_{t\to\infty} \mathbf{E}[\lambda_t] = \frac{\alpha\bar{\lambda}_i}{\alpha - \sum_{j=1}^m \delta_{ij}\int_{\mathbb{R}} y\, dF^j(y)}$$

and

$$\lim_{t\to\infty} \mathbf{E}[\lambda_t] = \frac{\alpha\bar{\lambda}_i}{\alpha - \sum_{j=1}^m \delta_{ij}},$$

respectively.

We only consider contagious jump specifications in this work. Simultaneous jumps can without loss of tractability be included to the dynamics in (4), but is not considered here in order to keep the number of parameters at a reasonable level.

To ensure absence of arbitrage, we impose the martingale condition on the price dynamics via the drift[1]

$$\mu_t^i = -\frac{1}{2}V_t^i - \lambda_t^i \int_{\mathbb{R}} (e^y - 1) dF^i(y) = -\frac{1}{2}V_t^i - \lambda_t^i \xi_i, \tag{8}$$

where

$$\xi_i = \int_{\mathbb{R}} (e^y - 1)\, dF^i(y).$$

Fig. 2 depicts simulated sample paths of four different indexes and their respective paths of volatilities and intensities for the intensity specification of Eq. (2) coupled with negative exponential jumps in returns. Notice how a jump in one index is reflected in jumps in both its own intensity as well as the other index intensities.

2.3. Characteristic function

The solution to the SDE in (4) is given by

$$X_t^i = \int_0^t \mu_s^i ds + \int_0^t \sqrt{V_s^i} dW_s^i + J_t^i. \tag{9}$$

We are interested in the time-t conditional characteristic function for the processes X^i for $i = 1,\dots,m$ in a future time point T

$$\psi^i(u,t,T) = \mathbb{E}\left[e^{iuX_T^i}|\mathcal{F}_t\right] \tag{10}$$
$$X_0 = 0,$$

as knowledge of this enables efficient pricing of European options via Fourier transform methods (Carr and Madan, 1999; Lewis, 2001). Using independence of the driving processes we can split the characteristic function into two parts

$$\begin{aligned}\psi^i(u,t,T) &= \mathbb{E}\left[e^{iu\left(-\frac{1}{2}\int_0^T V_s^i ds + \int_0^T \sqrt{V_s^i} dW_s^i\right)}|\mathcal{F}_t\right]\mathbb{E}\left[e^{iu\left(-\xi_i\int_0^T \lambda_s^i ds + J_T^i\right)}|\mathcal{F}_t\right] \\ &= \psi_1^i(u,t,T)\psi_2^i(u,t,T),\end{aligned} \tag{11}$$

[1] The drift condition ensures that the discounted asset prices are local martingales. However, verifying conditions given in Kallsen and Muhle-Karbe (2010) reveals that the discounted asset prices are true martingales for the specifications considered. The reader is referred to Appendix B for more details.

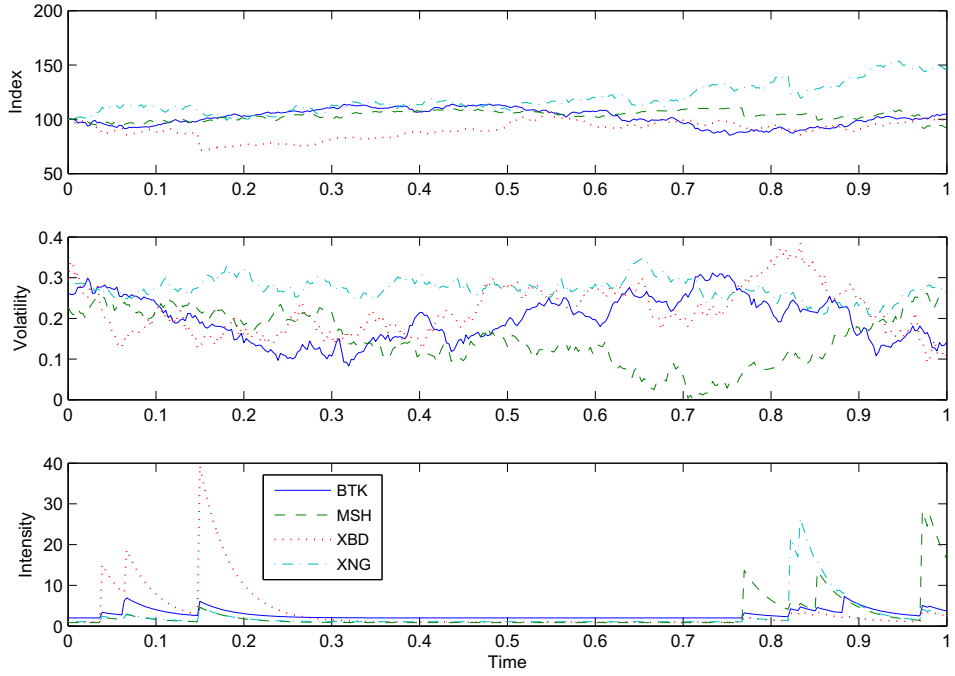

Fig. 2. Sample paths of the prices, volatilities, and jump intensities of the four indexes simulated from the negative exponential jump specification described in Section 2.4.1 with parameters calibrated to the option markets on September 21, 2009. The parameters are reported in Section 3.4.

where ψ_1^i and ψ_2^i refer to the characteristic functions of the Heston stochastic variance part and the part driven by the jump process, respectively.

2.3.1. Characteristic function of the Heston process

For the first part, $\psi_1^i(u,t,T)$ is equal to the characteristic function in the Heston (1993) model written here in the form given in Schoutens et al. (2004) and Gatheral (2006)

$$\psi_1^i(u,t,T) = \exp\left\{C_i(u,t,T)\overline{V}_i + D_i(u,t,T)V_t^i\right\} \times \exp\left\{iu\left(-\frac{1}{2}\int_0^t V_s^i ds + \int_0^t \sqrt{V_s^i}dW_s^i\right)\right\}, \tag{12}$$

where

$$C_i(u,t,T) = \frac{\kappa_i}{\eta_i^2}\left((m_i - d_i)(T-t) - 2\log\frac{1-g_i e^{-d_i(T-t)}}{1-g_i}\right) \tag{13}$$

$$D_i(u,t,T) = \frac{1}{\eta_i^2}(m_i - d_i)\frac{1-e^{-d_i(T-t)}}{1-g_i e^{-d_i(T-t)}}, \tag{14}$$

and

$$m_i = \kappa_i - \eta_i\rho_i ui, \quad d_i = \sqrt{m_i^2 + \eta_i^2(ui + u^2)}, \quad g_i = \frac{m_i - d_i}{m_i + d_i}.$$

2.3.2. Characteristic function of the mutually self-exciting process

Let $\underline{\mathbf{0}}$ denote a $1\times m$-dimensioned vector of zeros, $\underline{\underline{\mathbf{0}}}$ an $m\times m$ matrix of zeros and e_i the unit vector, a $1\times m$ vector with 1 at the i'th entry and zeros at all other entries. The process

$$Y_t = \left[\lambda_t^1 \quad \dots \quad \lambda_t^m \quad -\xi_1\int_0^t \lambda_s^1 ds + J_t^1 \quad \dots \quad -\xi_m\int_0^t \lambda_s^m ds + J_t^m\right]^\top = \left[\underline{\lambda}_t \quad \underline{J}_t\right]^\top \tag{15}$$

is a $2m$-dimensioned affine process (see Proposition 4.4 in Errais et al. (2010)) with coefficients

$$K_0 = \left[\alpha_1\bar{\lambda}_1 \quad \dots \quad \alpha_m\bar{\lambda}_m \quad \underline{\mathbf{0}}\right]^\top, \quad K_1 = \begin{bmatrix}\mathrm{diag}(-\alpha_1,\dots,-\alpha_m) & \underline{\underline{\mathbf{0}}} \\ \mathrm{diag}(-\xi_1,\dots,-\xi_m) & \underline{\underline{\mathbf{0}}}\end{bmatrix}$$
$$\Lambda_0^i = 0, \quad \Lambda_1^i = [e_i \quad \underline{\mathbf{0}}]^\top, \quad \zeta^i = \mathrm{diag}(\delta_{1,i},\dots,\delta_{m,i},e_i), \tag{16}$$

for $i = 1,\dots,m$. Since there is no Gaussian term in Y the volatility coefficients H_0 and H_1 are both populated with zeros.

For $v\in\mathbb{C}^{2m}$ the extended transform of the process Y is given by (see Proposition 1 in Duffie et al. (2000))

$$\Psi(v,Y_t,t,T) = \mathbb{E}\left[e^{v\cdot Y_T}|\mathcal{F}_t\right] = \exp\left(a(v,t,T) + b(v,t,T)\cdot Y_t\right), \tag{17}$$

where $a(t) = a(v,t,T)$ and $b(t) = b(v,t,T)$ satisfy the ODEs

$$\partial_t b(t) = -K_1^\top b(t) - \sum_{i=1}^m \Lambda_1^i\left(\theta^i\left(\zeta^i b(t)\right) - 1\right) \tag{18}$$

$$\partial_t a(t) = -K_0\cdot b(t), \tag{19}$$

with the boundary conditions $a(T) = 0$ and $b(T) = v$. θ^i is given by

$$\theta^i(\omega) = \int_{\mathbb{R}^{2m}} e^{\omega\cdot z}d\underline{F}^i(\underline{z}), \quad \omega\in\mathbb{C}^{2m}. \tag{20}$$

In the specifications of this paper the ODEs are solved numerically using the Runge–Kutta algorithm.

Let $u\in\mathbb{R}$ and define

$$u_i = [\underline{\mathbf{0}} \quad uie_i]^\top.$$

The characteristic function driven by the jump process for asset i can then be computed using the extended transform as

$$\psi_2^i(u,t,T) = \Psi(u_i,Y_t,t,T). \tag{21}$$

2.4. Parametric examples

In this section the two model specifications considered in the paper are introduced and the resulting ODEs in Eqs. (18) and (19) are detailed.

2.4.1. Negative exponential jumps and jump size dependent intensities

Let $\underline{\mathbf{1}}$ denote a $1 \times m$ vector of ones and define the pure jump process entering Eq. (1) as a $2m$-dimensioned replica of J^i

$$\underline{J}_t^i = J_t^i[\underline{\mathbf{1}} \quad \underline{\mathbf{1}}]^\top. \tag{22}$$

With this specification the jumps in the intensities are proportional to the jumps in the asset returns as in (2). We will let the jump size distributions F^is have support on $(-\infty, 0]$ and take $\delta_{i,j} \leq 0$ in order to ensure non-negative intensities. If we take F^i as the negative exponential distribution with parameter $\gamma_i \in (0, \infty)$

$$dF^i(z) = \begin{cases} \gamma_i e^{\gamma_i z} dz & \text{for} \quad z \leqslant 0 \\ 0 & \text{for} \quad z > 0, \end{cases} \tag{23}$$

then

$$\theta^i\left(\zeta^i b(t)\right) = \int_{\mathbb{R}} \exp\left\{\left(\left(\zeta^i b(t)\right)_1 + \cdots + \left(\zeta^i b(t)\right)_{2m}\right) z\right\} dF^i(z) = \frac{\gamma_i}{\delta_{1,i} b_1(t) + \cdots + \delta_{m,i} b_m(t) + b_{m+i}(t) + \gamma_i}$$

$$\xi_i = \frac{\gamma_i}{1+\gamma_i} - 1,$$

where we in the first equality have used that $d\underline{F}^i(\underline{z}) = 0$ when the components $z_1, \ldots, z_{2m}$ of $\underline{z}$ are not identical and $d\underline{F}^i(\underline{z}) = dF^i(z)$ for $z_1 = \ldots = z_{2m} = z$. Hence, the ODEs in Eqs. (18) and (19) reduce to

$$\partial_t b_j(t) = \alpha_j b_j(t) + \xi_j b_{m+j}(t) - \frac{\gamma_j}{\delta_{1,j} b_1(t) + \cdots + \delta_{m,j} b_m(t) + b_{m+j}(t) + \gamma_j} + 1, \quad j = 1, \ldots, m$$

$$\partial_t b_j(t) = 0, \quad j = m+1, \ldots, 2m$$

$$\partial_t a(t) = -\alpha_1 \bar{\lambda}_1 b_1(t) - \cdots - \alpha_m \bar{\lambda}_m b_m(t).$$

with boundary conditions $a(T) = 0$ and $b(T) = v$. From the boundary condition we conclude that $b_j(t) = v_j$ for $j = m+1, \ldots, 2m$ and for all $t \leqslant T$.

2.4.2. Gaussian jumps

We also consider an example of the intensity specification (3) and define

$$\underline{J}_t^i = \left[N_t^i \underline{\mathbf{1}} \quad J_t^i \underline{\mathbf{1}}\right]^\top, \tag{24}$$

where the first m entries are the counting process for jumps in asset i and the last m entries the cumulative sum of jumps of asset i. To allow for both positive and negative jumps in asset returns we consider Gaussian jumps with mean $\beta_i \in (-\infty, \infty)$ and standard deviation $\sigma_i \in (0, \infty)$ and take

$$dF^i(z) = \frac{1}{\sigma_i \sqrt{2\pi}} e^{-\frac{(z-\beta_i)^2}{2\sigma_i^2}} dz. \tag{25}$$

In this case we get

$$\theta^i\left(\zeta^i b(t)\right) = \int_{\mathbb{R}} e^{(\zeta^i b(t))_1 + \cdots + \left(\zeta^i b(t)\right)_m + \left(\left(\zeta^i b(t)\right)_{m+1} + \cdots + \left(\zeta^i b(t)\right)_{2m}\right) z} dF^i(z) = e^{\delta_{1,i} b_1(t) + \cdots + \delta_{m,i} b_m(t) + b_{m+i}(t)\beta_i + \frac{1}{2} b_{m+i}(t)^2 \sigma_i^2}$$

$$\xi_i = e^{\beta_i + \frac{1}{2}\sigma_i^2} - 1,$$

where the first equation follows by using that the jump sizes of N_t^i are known and equal to 1. I.e. $d\underline{F}^i(\underline{z}) = dF^i(z)$ for $z_1 = \cdots = z_m = 1$ and $z_{m+1} = \cdots = z_{2m} = z$ and $d\underline{F}^i(\underline{z}) = 0$ elsewhere. The ODEs reduce to

$$\partial_t b_j(t) = \alpha_j b_j(t) + \xi_j b_{m+j}(t) - e^{\delta_{1,j} b_1(t) + \cdots + \delta_{m,j} b_m(t) + b_{m+j}(t)\beta_j + \frac{1}{2} b_{m+j}(t)^2 \sigma_j^2} + 1, \quad j = 1, \ldots, m$$

$$\partial_t b_j(t) = 0, \quad j = m+1, \ldots, 2m$$

$$\partial_t a(t) = -\alpha_1 \bar{\lambda}_1 b_1(t) - \cdots - \alpha_m \bar{\lambda}_m b_m(t).$$

with boundary conditions $a(T) = 0$ and $b(T) = v$. In this case we also see that $b_j(t) = v_j$ for $j = m+1, \ldots, 2m$ and for all $t \leqslant T$.

2.5. Extracting the joint probability distribution from the characteristic function

We start by analyzing the univariate density function. Knowledge of the characteristic function of X_T^i is essentially the same as knowing the probability density function of the log-returns $f_{X_T^i}$ by the inverse Fourier transform of the characteristic function

$$f_{X_T^i}(z; t) = \frac{1}{2\pi} \int_{-\infty}^{\infty} e^{-iuz} \psi^i(u, t, T) du. \tag{26}$$

In Fig. 3 probability density functions for the log-returns in the negative exponential jump specification are depicted in three scenarios, where the base case model parameters are reported in Section 3.4 and the result of a calibration to the index option surfaces on September 21, 2009. All three density functions correspond to the BTK index, but differ in their cross-contagion parameters:

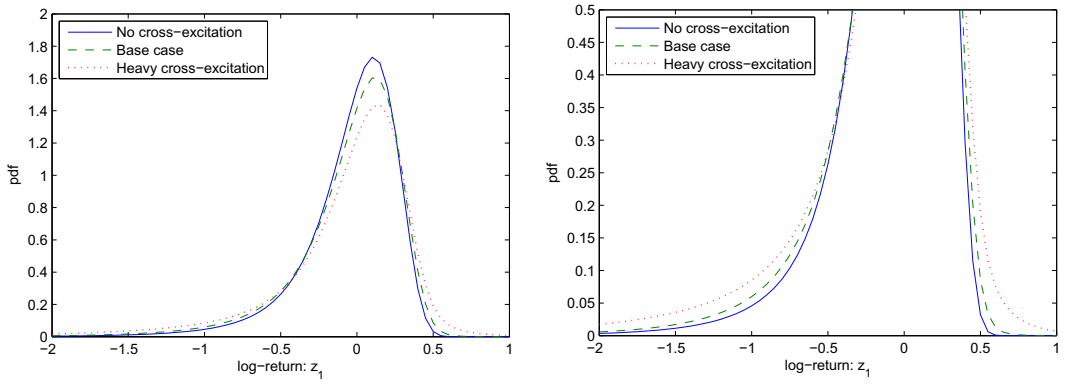

Fig. 3. Univariate probability density functions for the log-return process of the BTK index over a horizon of 1 year for three different levels of contagion in the negative exponential jump specification. The right graph shows the same graph as the left but on a larger scale for the y-axis.

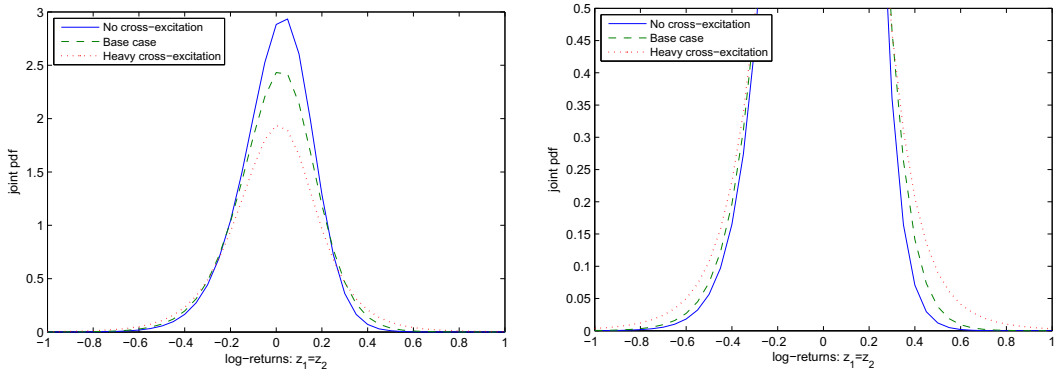

Fig. 4. Bivariate probability density functions for the log-return processes of the BTK and the MSH indexes over a horizon of 1 year for three different levels of contagion along the line $z_1 = z_2$ in the negative exponential jump specification. The right graph shows the same graph as the left but on a larger scale for the y-axis.

1. No cross-excitation: The base scenario but without any cross-excitation. Hence, $\delta_{ij} = 0$ for $i \neq j$.
2. The base scenario: calibrated parameters to the four index option surfaces on September 21, 2009.
3. Heavy cross-excitation: The base scenario but with all cross excitation-parameters multiplied by 2.[2]

We observe how the contagion parameters have two effects on the law of the log-returns. First, increasing the contagion leads to thicker tails of the distribution. Second, increasing the contagion leads to more negatively skewed distributions.

Similar to the univariate case we have a relation like Eq. (26) for the multivariate case $X = \left(X^1, \ldots, X^m\right)$ (Shephard, 1991), which relates the joint characteristic function to the joint law of the log-returns

$$f_{X_T}(z;t) = \frac{1}{(2\pi)^m} \int_{\mathbb{R}^m} e^{-\mathrm{i}z'\underline{u}} \psi_1^1(u_1,t,T) \times \cdots \times \psi_1^m(u_m,t,T) \Psi(v,Y_t,t,T) d\underline{u}, \tag{27}$$

where $\underline{u} \in \mathbb{R}^m$ and

$$v = [\underline{0} \quad \underline{u}\mathrm{i}]. \tag{28}$$

To see how the contagion impacts the joint law of the index returns, Fig. 4 depicts the joint density function of the BTK and MSH indexes in the three contagion scenarios along the line $z_1 = z_2$. We see how increasing the contagion also leads to fatter tails in the joint density making it more likely to observe high joint losses or high joint gains.

3. Calibration of the model specifications

In this section we assess the pricing performance of the models by calibrating them to the four selected index options surfaces. First we give a description of the data. Next, we describe the calibration approach in detail in Section 3.2. In Section 3.3 the robustness of the proposed calibration approach is studied before implementing the model specifications on the options data in Section 3.4. Finally, the pricing performance of the models are studied over an extended period of time in Section 3.5.

3.1. Data description

We asses the model performances on an options data set running from April 9, 2007 to September 21, 2009, a total of 611 days. On each date we have call and put options data for 4 or 5 maturities for the four indexes: BTK ($i = 1$), MSH ($i = 2$), XBD ($i = 3$), and XNG ($i = 4$). The indexes are suitable for two reasons: First, they represent four major sectors of the economy, and Second, they have no overlapping company names. The options are all traded on the NASDAQ options exchange and their quotes are collected from OptionMetrics. As the option price we use the mid of the quoted closing bid-ask prices. In order to ensure that the data used for the calibrations are reliable, we filter the data in a number of ways: option quotes where either the bid price is zero or the call/put bid-price is so low that the corresponding put/call bid-price derived via the put-call parity is negative, options with absolute moneyness $|\frac{K}{S} - 1| > 0.40$, options with remaining time to maturity less than a calendar week, or options with a nominal bid-ask spread greater than \$5 have been filtered out. Compared to many existing studies (e.g. Bakshi et al., 1997; Kaeck, 2013; Madan, 2011) we calibrate to options within a wide range of moneyness, since far out of the money options are essential in estimating jump parameters, as these contain most information about the tails of the return distribution. Next, we only calibrate to options with strikes, where both the put and call prices are quoted. When this is the case we convert the put price to a call price via the put-call parity and compute the average of the two available call prices.[3]

On this set of call prices, we filter away observations that violate the no-arbitrage bounds (Carr and Madan, 2005; Cousot, 2007)

$$C_t(S_t;T,K_j) > \max\left\{0, S_t e^{-\int_t^T q_s ds} - K_j e^{-\int_t^T r_s ds}\right\} \tag{29}$$

$$\frac{C_t(S_t;T,K_{j-1}) - C_t(S_t;T,K_j)}{K_j - K_{j-1}} \in \left[0, e^{-\int_t^T r_s ds}\right] \tag{30}$$

$$\frac{C_t(S_t;T,K_{j-1}) - C_t(S_t;T,K_j)}{K_j - K_{j-1}} - \frac{C_t(S_t;T,K_j) - C_t(S_t;T,K_{j+1})}{K_{j+1} - K_j} \geqslant 0, \tag{31}$$

where $K_{j-1} < K_j < K_{j+1}$. We only calibrate to a given index option surface if we have more than 10 available quotes after the filtering is performed. The prices of the underlying index and the options are closing quotes of each day in the sample. We use the US discount curve provided by OptionMetrics, and the constant and continuously compounded dividend yield for each index is derived from put and call options around at-the-money using the put-call parity.

[2] The multiplication constant is chosen such that the stability constraints (6) and (7) are satisfied for both model specifications.

[3] This is not restrictive as, as both the put and call option quote are available in most cases. Additionally, we found that the resulting "average" call prices was violating the arbitrage constraints (29)–(31) on far less occasions compared to the case if we had used, e.g. only out of the money option quotes.

Table 1
Sample properties of the options on the four indexes. The reported numbers are the average bid-ask mid price, the average of the effective bid-ask spread (in parentheses), and the total number of observations in each moneyness-maturity category (in braces). The sample period runs from April 9, 2007 to September 21, 2009, a total of 611 days.

		Days to expiration			
Index	Moneyness K/S	$\leqslant 60$	60–180	>180	Subtotal
BTK	$\leqslant$0.90	121.75	156.16	180.29	
		(1.65)	(1.78)	(2.15)	
		{1901}	{5161}	{2845}	{9907}
	0.9–1.0	48.37	69.72	92.84	
		(1.66)	(1.96)	(2.21)	
		{4148}	{4402}	{1963}	{10513}
	1.0–1.1	11.89	26.86	50.22	
		(1.67)	(1.95)	(2.22)	
		{3504}	{4066}	{1936}	{9506}
	> 1.1	4.94	8.47	17.01	
		(1.77)	(1.78)	(2.14)	
		{696}	{4034}	{3275}	{8005}
Subtotal		{10249}	{17663}	{10019}	{37931}
MSH	$\leqslant$0.90	79.98	110.48	127.22	
		(1.34)	(1.49)	(1.58)	
		{2822}	{8484}	{5167}	{16473}
	0.9–1.0	34.74	50.29	66.17	
		(1.32)	(1.64)	(1.74)	
		{4844}	{5924}	{3095}	{13863}
	1.0–1.1	8.69	20.49	35.87	
		(1.32)	(1.62)	(1.74)	
		{4499}	{5795}	{3076}	{13370}
	> 1.1	3.54	6.47	13.19	
		(1.55)	(1.63)	(1.81)	
		{1347}	{6070}	{4408}	{11825}
Subtotal		{13512}	{26273}	{15746}	{55531}
XBD	$\leqslant$0.90	28.29	37.46	42.52	
		(0.95)	(1.12)	(1.39)	
		{1889}	{4497}	{2704}	{9090}
	0.9–1.0	13.29	18.77	24.21	
		(0.98)	(1.19)	(1.46)	
		{2500}	{2561}	{1205}	{6266}
	1.0–1.1	4.74	9.75	15.46	
		(0.95)	(1.19)	(1.48)	
		{2307}	{2453}	{1217}	{5977}
	> 1.1	2.16	4.00	6.59	
		(0.85)	(1.10)	(1.44)	
		{1290}	{4194}	{3129}	{8612}
Subtotal		{7986}	{13704}	{8255}	{29945}
XNG	$\leqslant$0.90	90.43	111.98	129.94	
		(1.73)	(2.02)	(2.23)	
		{1890}	{5353}	{2867}	{10110}
	0.9–1.0	36.84	52.69	70.73	
		(1.73)	(2.12)	(2.29)	
		{3268}	{3549}	{1564}	{8381}
	1.0–1.1	11.88	25.28	43.69	
		(1.74)	(2.14)	(2.30)	
		{3059}	{3508}	{1595}	{8162}
	> 1.1	6.02	10.88	20.4	
		(1.83)	(2.12)	(2.30)	
		{1320}	{4536}	{2795}	{8651}
Subtotal		{9537}	{16946}	{8821}	{35304}
Total					{158711}

Table 1 reports sample properties of the index option prices divided into different categories according to the moneyness and maturity of the options. The effective bid-ask spread is defined as the ask price deducted the bid-ask mid price.

3.2. Two-step calibration approach

On each date, calibration of the model is done in two steps in order to reduce computation time.

1. First, the parameters of the mutually self-exciting processes are calibrated for the indexes simultaneously.
2. Second, the Heston dynamics are calibrated on each index independently.

3.2.1. Calibration of the jump process

In the first step we assume the log-asset returns follow jump diffusive processes with

$$dX_t^i = \left(-\frac{1}{2}I_i^2 - \lambda_t^i \xi_i\right)dt + I_i dW_t^i + dJ_t^i, \tag{32}$$

where I_i equals the minimum implied volatility in the set of options on index i. The joint asset dynamics are calibrated to the four most out-of-the-money call and put options for the four shortest maturities for the four indexes, a total of 128 prices when all quotes are available. Including the diffusion in the dynamics raises the model implied volatility to the level I_i. A calibration of the pure jump model with no diffusion would result in extreme values for the jump parameters and leave little freedom to calibrate the Heston dynamics to the individual surfaces in the next step.

Utilizing the characteristic function in Eq. (11), the model option prices are computed using the Fourier transform formula of Lewis (2001)

$$C_t(S_t^i, K) = S_t^i e^{-\int_t^T q_s^i ds} - \frac{\sqrt{S_t^i K} e^{-\frac{\int_t^T (r_s + q_s^i)ds}{2}}}{\pi} \int_0^\infty \frac{\mathcal{R}\left(e^{iuk_i}\psi^i\left(u - \frac{i}{2}, t, T\right)\right)}{u^2 + \frac{1}{4}} du, \tag{33}$$

where $k_i = \log\left(\frac{S_t}{K}\right) + \int_t^T r_s - q_s^i ds$. In order to make the calibration more robust we apply the technique suggested in Andersen and Andreasen (2002), where the distribution of log-returns is approximated by a normal and the payoff transform (33) is integrated against the difference of model transforms after which the Black–Scholes price is added to get the correct model price.

The calibration is performed by minimizing the Sum of Squared Errors (SSE) on model and market implied volatilities across maturities and strikes of the selected option quotes.

Table 2
Calibrated parameters from the computed option prices with the negative exponential and the Gaussian jumps size specification.

	κ	$\overline{V}$	η	V_0	ρ	α	$\bar{\lambda} = \lambda_0$	$\delta_{i,i}$	δ_{cross}	γ	σ	β	ARPE (%)
Negative exponential													
True	3	0.01	1	0.01	−0.6	40	1	−200	−20	15	–	–	–
Calibration	5.5	0.005	0.83	0.011	−0.53	42.1	0.69	−190	−52.6	13.3	–	–	1.89
Gaussian													
True	3	0.01	1	0.01	−0.6	40	1	15	2	–	0.1	−0.1	–
Calibration	8.7	0.015	1.3	0.014	−0.49	36.6	0.56	13.1	1.6	–	0.12	−0.14	1.78

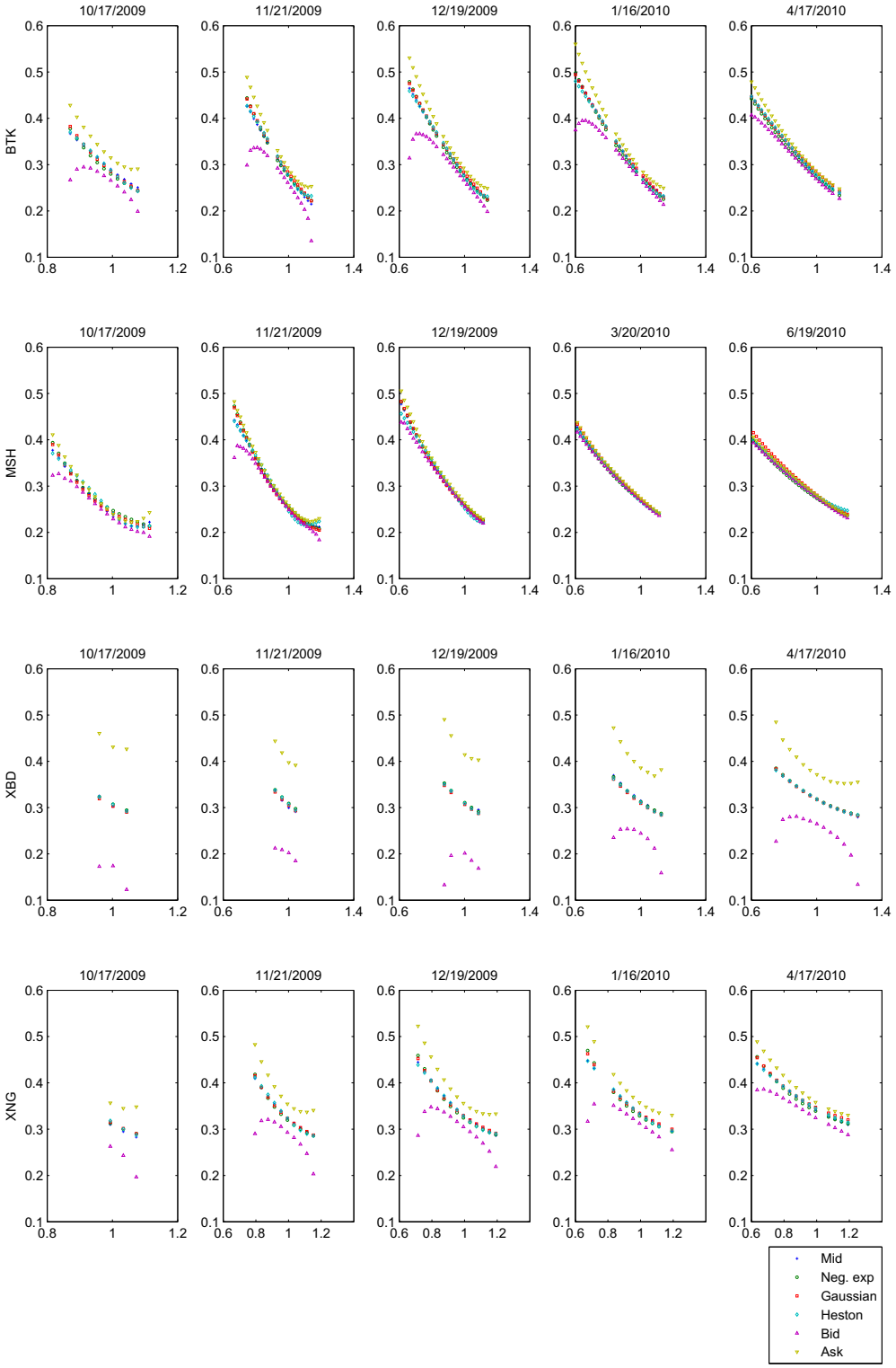

Fig. 5. Fit of the models to the options smiles on September 21, 2009 of the four indexes. The moneyness $m = K/F_t^T$ is along the x-axis and the implied volatility along the y-axis.

$$\text{SSE} = \sum_{\text{options}} \left(I^{Market} - I^{Model}\right)^2, \tag{34}$$

using a gradient-based minimization algorithm. We impose Eqs. (6) and (7) by introducing a positive parameter in the calibration given by

$$H_i = \alpha_i - \sum_{j=1}^{m} \delta_{i,j} \int_{\mathbb{R}} y \, dF^j(y) > 0 \tag{35}$$

$$H_i = \alpha_i - \sum_{j=1}^{m} \delta_{i,j} > 0, \tag{36}$$

from which α_i is implied. It is preferable to calibrate the models based on a distance criteria between model and market implied volatilities as in (34) since the absolute value of the indexes are different. Hence, we would put more weight on options on the index with the greatest value if the more standard choice of the sum of squared differences of option prices was used as objective function.

3.2.2. Calibration of the Heston parameters

Once the parameters of the jump processes are determined, the parameters in the Heston characteristic function (12) can be calibrated independently for each index to the options data for all maturities. It is crucial to include the stochastic volatility component as this enables the fit of the model to the individual surfaces.

3.3. Robustness of the calibration procedure

In this section we compute a set of option prices for a number of strikes and maturities with a given set of parameter values. Then we invert the computed option prices using the described calibration approach to check the robustness of the approach. For simplicity we consider a symmetric market with four indexes normalized at initial value 100 having the same dynamics and the same number of options with similar characteristics, i.e. same strikes and maturities. Furthermore, we also put $\bar{\lambda}_i = \lambda_0^i$ for all $i,j = 1,\dots,m$. The parameters for the two specifications are reported in the rows that say "'true" of Table 2. The parameters are chosen so that the resulting implied volatility surfaces are at a realistic level, but otherwise arbitrarily. Besides checking the robustness, the model calibrations are compared via the Average Relative Pricing Error (ARPE) defined as

$$\text{ARPE} = \frac{1}{\#\{\text{options}\}} \sum_{\text{options}} \frac{|\, I_{Calibration} - I_{True} \,|}{I_{True}}. \tag{37}$$

For many of the parameters, the calibration returns values that are not too far away from the true values. However, the speed of the mean reversion κ, the long-run variance $\overline{V}$, and the cross excitation parameter δ_{cross} seem to be particular difficult to calibrate. Often whenever one wishes to calibrate a model including both stochastic volatility and jumps, identification of the parameters can be problematic as e.g. negative skewness in the distribution can be achieved by both negative correlation between the driving Wiener processes or via the jump distribution. If the model is required to be used more dynamically than in the present work, a practical solution would be to fix some of the parameters in the calibration, or to include a relative entropy term in the objective function as proposed in Cont and Tankov (2004). Additionally, difficulties in identifying the cross contagion parameter come as no surprise as the models are calibrated to single name options, which does not reveal information about the correlation/contagion between indexes. Ideally, one should include multi-name derivatives in the calibration in order to identify the contagion parameters, but has not been done in this work due to lack of data.

3.4. Calibration performance on a single date

Here we calibrate the models to options data from September 21, 2009. We use the Heston model as benchmark in order to assess the performance of the model specifications. Again we compare the models by computing the ARPE defined in Eq. (37) with I_{True} exchanged with the implied volatility of the mid bid-ask price observed in the market I_{Mid}. As it is of interest to see how well the models fit within the bid-ask spread we also report the Average Relative Bid-Ask Error (ARBAE) defined as

$$\text{ARBAE} = \frac{1}{\#\{\text{options}\}} \sum_{\text{options}} \frac{\max\left\{(I_{Calibration} - I_{Ask})^+, (I_{Bid} - I_{Calibration})^+\right\}}{I_{Mid}}. \tag{38}$$

The Heston models are calibrated to each options market independently, while the other two specifications are 4-dimensional multivariate models that are calibrated simultaneously to the four options markets.

In step 1) of the calibration of the negative exponential jump specification we make a number of parameter reductions by putting $H_i = H_j, \delta_{i,i} = \delta_{j,j}, \bar{\lambda}_i = \lambda_0^i$ for all $i,j = 1,\dots,m$ and $\delta_{i,j} = \delta_{cross}$ for all $i \neq j$. Hence, in the calibration only the parameters determining the mean jump size γ_i and the intensity of the jumps in the short and long run $\bar{\lambda}_i = \lambda_0^i$ are allowed to be index specific. Similar for the Gaussian jump specification, we make the same reductions in the intensity parameters as above and also set $\sigma_i = \sigma_j$ for all $i,j = 1,\dots,m$. Again, only the mean jump sizes β_i and $\bar{\lambda}_i = \lambda_0^i$ are allowed to be index specific. We impose the stability restrictions (6) and (7) and put $\alpha_i = H_i + \sum_{j=1}^m \delta_{i,j} \int_{\mathbb{R}} y\, dF^j(y)$ and $\alpha_i = H_i + \sum_{j=1}^m \delta_{i,j}$ for the two specifications, respectively. In the second step 2) we allow all the parameters in the Heston dynamics to be index specific.

Fig. 5 depicts the fits of the three models to the volatility smiles of the four indexes as a function of the forward moneyness K/F_t^T,

Table 3
September 21, 2009 calibrated parameters for the three model specifications for the four indexes. The ARPEs are reported in percentage, while the ARBAEs are reported in basis points.

	κ	$\overline{V}$	η	V_0	ρ	α	$\bar{\lambda} = \lambda_0$	$\delta_{i,i}$	δ_{cross}	γ	σ	β	ARPE	ARBAE
Heston														
BTK ($i=1$)	2.47	0.129	1.31	0.087	−0.63								1.15	0
MSH ($i=2$)	4.04	0.119	1.42	0.061	−0.57								1.53	40
XBD ($i=3$)	2.73	0.143	0.89	0.095	−0.55								0.80	0
XNG ($i=4$)	4.73	0.161	1.30	0.099	−0.54								0.78	0
Neg. exp. jumps														
BTK ($i=1$)	5.78	0.025	0.39	0.069	−0.84	25.9	1.99	−187	−18	12.4			1.19	0
MSH ($i=2$)	0.83	0.058	0.38	0.052	−0.60	26.4	0.84	–	–	12.0			0.96	7
XBD ($i=3$)	6.54	0.067	0.59	0.087	−0.49	27.5	0.96	–	–	11.1			0.74	0
XNG ($i=4$)	11.91	0.077	0.35	0.085	−0.76	29.6	1.06	–	–	9.8			1.21	0
Gaussian jumps														
BTK ($i=1$)	5.56	0.021	0.39	0.068	−0.74	20.8	1.13	13.5	1.1		0.057	−0.140	1.07	0
MSH ($i=2$)	1.98	0.046	0.38	0.054	−0.63	–	0.29	–	–		–	–0.183	1.18	16
XBD ($i=3$)	6.08	0.067	0.61	0.089	−0.46	–	0.38	–	–		–	−0.181	0.81	0
XNG ($i=4$)	9.39	0.074	0.45	0.086	−0.52	–	0.61	–	–		–	−0.185	1.07	0

Table 4
The table reports the ARPE and the ARBAE (in parentheses) for different levels of moneyness and maturity across the observation dates for the four indexes and the three models. The ARPEs are reported in percentage, while the ARBAEs are reported in basis points.

			Days to expiration			
Index	Moneyness K/S	Model	$\leqslant 60$	60–180	> 180	All
BTK	$\leqslant$0.90	Heston	2.03 (1)	1.37 (1)	1.09 (2)	1.42 (1)
		Neg. exp.	4.21 (12)	2.10 (4)	2.14 (17)	2.51 (9)
		Gaussian	4.02 (10)	1.93 (3)	2.25 (19)	2.42 (9)
	0.9–1.0	Heston	2.60 (6)	1.24 (1)	1.14 (6)	1.76 (4)
		Neg. exp.	2.79 (7)	1.32 (2)	1.74 (23)	1.98 (8)
		Gaussian	2.84 (8)	1.35 (2)	1.62 (17)	1.99 (7)
	1.0–1.1	Heston	3.06 (9)	1.87 (4)	1.14 (4)	2.16 (6)
		Neg. exp.	2.50 (4)	1.57 (3)	1.35 (18)	1.87 (6)
		Gaussian	2.52 (4)	1.56 (3)	1.30 (16)	1.86 (6)
	>1.1	Heston	3.02 (3)	2.53 (4)	1.88 (2)	2.31 (3)
		Neg. exp.	3.07 (7)	2.29 (10)	1.66 (24)	2.10 (15)
		Gaussian	3.07 (7)	2.24 (11)	1.68 (27)	2.09 (17)
	All	Heston	2.68 (6)	1.72 (2)	1.37 (3)	1.89 (3)
		Neg. exp.	2.97 (7)	1.82 (5)	1.75 (21)	2.12 (9)
		Gaussian	2.96 (7)	1.77 (5)	1.76 (21)	2.09 (10)
MSH	$\leqslant$0.90	Heston	2.53 (2)	1.51 (0)	1.04 (1)	1.54 (1)
		Neg. exp.	4.37 (24)	1.88 (2)	1.61 (6)	2.22 (7)
		Gaussian	4.16 (19)	1.77 (2)	1.56 (4)	2.11 (6)
	0.9–1.0	Heston	3.95 (45)	1.70 (7)	1.18 (3)	2.37 (19)
		Neg. exp.	3.52 (19)	2.18 (10)	1.26 (16)	2.44 (15)
		Gaussian	3.50 (19)	2.06 (10)	1.21 (12)	2.37 (14)
	1.0–1.1	Heston	4.05 (45)	2.44 (24)	1.91 (21)	2.86 (31)
		Neg. exp.	3.43 (21)	1.73 (5)	1.63 (31)	2.28 (17)
		Gaussian	3.38 (20)	1.71 (5)	1.61 (28)	2.25 (15)
	>1.1	Heston	2.97 (1)	2.25 (3)	2.77 (27)	2.53 (12)
		Neg. exp.	3.28 (3)	2.01 (12)	2.71 (68)	2.41 (32)
		Gaussian	3.18 (3)	2.05 (14)	2.70 (68)	2.42 (33)
	All	Heston	3.59 (32)	1.93 (8)	1.72 (12)	2.27 (15)
		Neg. exp.	3.64 (19)	1.95 (7)	1.85 (31)	2.33 (17)
		Gaussian	3.56 (18)	1.88 (7)	1.82 (28)	2.27 (16)
XBD	$\leqslant$0.90	Heston	1.96 (0)	1.38 (0)	1.40 (1)	1.51 (0)
		Neg. exp.	2.32 (0)	1.60 (1)	2.02 (5)	1.88 (2)
		Gaussian	2.24 (0)	1.53 (1)	1.85 (3)	1.77 (1)
	0.9–1.0	Heston	2.55 (3)	1.36 (1)	1.02 (0)	1.77 (1)
		Neg. exp.	2.00 (1)	1.47 (1)	1.60 (8)	1.71 (2)
		Gaussian	1.97 (1)	1.36 (1)	1.63 (8)	1.65 (2)
	1.0–1.1	Heston	3.34 (4)	2.10 (3)	1.00 (0)	2.36 (3)
		Neg. exp.	2.26 (1)	1.38 (1)	1.47 (11)	1.74 (3)
		Gaussian	2.24 (1)	1.39 (1)	1.57 (11)	1.76 (3)
	>1.1	Heston	2.49 (1)	2.12 (2)	2.13 (3)	2.18 (2)
		Neg. exp.	2.50 (1)	1.74 (1)	2.28 (17)	2.05 (7)
		Gaussian	2.43 (1)	1.75 (2)	2.25 (16)	2.02 (7)
	All	Heston	2.63 (2)	1.73 (1)	1.56 (1)	1.92 (2)
		Neg. exp.	2.24 (1)	1.58 (1)	1.98 (11)	1.86 (4)
		Gaussian	2.19 (1)	1.54 (1)	1.93 (10)	1.82 (3)
XNG	$\leqslant$0.90	Heston	1.39 (0)	0.99 (0)	0.96 (0)	1.06 (0)
		Neg. exp.	2.28 (0)	1.60 (0)	1.27 (0)	1.63 (0)
		Gaussian	2.10 (0)	1.54 (0)	1.27 (0)	1.57 (0)
	0.9–1.0	Heston	1.77 (1)	0.97 (0)	1.01 (0)	1.29 (0)
		Neg. exp.	1.67 (0)	1.16 (0)	0.80 (0)	1.29 (0)
		Gaussian	1.65 (0)	1.12 (0)	0.76 (0)	1.26 (0)
	1.0–1.1	Heston	2.60 (3)	1.59 (0)	1.20 (2)	1.90 (2)
		Neg. exp.	1.72 (0)	0.94 (0)	0.85 (1)	1.21 (0)
		Gaussian	1.72 (0)	0.96 (0)	0.87 (1)	1.23 (0)
	>1.1	Heston	1.90 (0)	1.43 (0)	1.60 (1)	1.56 (1)
		Neg. exp.	1.69 (0)	0.97 (0)	1.30 (3)	1.18 (1)
		Gaussian	1.67 (0)	0.99 (0)	1.29 (4)	1.19 (1)
	All	Heston	1.98 (1)	1.23 (0)	1.21 (1)	1.43 (1)
		Neg. exp.	1.81 (0)	1.20 (0)	1.12 (1)	1.35 (0)
		Gaussian	1.77 (0)	1.18 (0)	1.11 (1)	1.32 (0)

where $F_t^T = S_t e^{\int_t^T (r_s - q_s)ds}$. It is clear that all the models are able to achieve a satisfactory fit to the market.

Table 3 reports the calibrated parameters for the three models. We observe how the three models perform satisfactory when assessed according to both error measures. When evaluated using the ARBAE measure the two contagion specifications perform better than the Heston model, since the latter overprices the longest maturity MSH options slightly.

Note that α varies in the negative exponential jump specification due to the dependency on γ_i in (35).

3.5. Calibration performance over an extended period of time

In this section we calibrate the models to options data over the period from April 9, 2007 to September 21, 2009, a total of 611 days. Again we benchmark the two contagion specifications

against the Heston model, and the models are re-calibrated each day with the procedure described in Section 3.4.

The function defined in Eq. (34) is the minimization objective in all the calibrations and we compare the models via the ARPE and ARBAE measures. To assess the model performances we compare the pricing errors across calendar dates for different levels of moneyness-maturity categories, namely far ITM calls with $0.6 \leqslant K/S \leqslant 0.90$, ITM calls with $0.9 < K/S \leqslant 1.0$, OTM calls with $1.0 < K/S \leqslant 1.1$, and finally far OTM calls defined as options with moneyness in the interval $1.1 < K/S \leqslant 1.4$. Moreover, we also divide the options into three categories according to their time to expiration; short maturity options with 7 days $< T - t \leqslant 60$ days, medium maturity options with 60 days $< T - t \leqslant 180$ days, and long maturity options with $T - t > 180$ days.

On each index and for each model, Table 4 reports the error measures ARPE and ARBAE for the different categories of the maturity-moneyness across calendar dates.

When comparing both error measures based on all the options the models perform well with none of the models being a clear winner, although measured by the overall ARPE the Gaussian jump specification perform slightly better than the negative exponential jump model for all the indexes. Interestingly, another picture emerges when considering the far ITM call options as the Heston model performs better for all the indexes. This is particular evident in the far ITM-short maturity options on the BTK and the MSH indexes, where the contagion specifications have close to twice the ARPE compared to the Heston model. This result is due to the parameter reductions performed and the fixing of the jump distribution in the first step of the calibration procedure. If some of the index options exhibit a steep implied volatility skew while others are more flat, this can result in too steep skews for the indexes with less pronounced IV skews. Obviously, if no parameter reductions where made and all the model parameters were calibrated simultaneously in one step, the contagion specifications would perform better than the embedded Heston model, but at the cost of a more complex optimization problem. When comparing the pricing errors on the OTM call options, the contagion specifications perform better than the Heston model in most cases, as the latter in general has difficulties generating enough curvature in the right wing of the smile. Overall they all perform well, but we stress here that the Heston models are calibrated independently, while the contagion specifications are multivariate models fitted simultaneously to all four option markets – a much more challenging task.

Looking at the error measures across the moneyness and maturity dimension in Table 4 maybe most surprising is the superior performance of the Heston model when it comes to the pricing of the short maturity and far in-the-money call options on the BTK and MSH indexes. In general the implied volatility smiles are more flat for the pre-crisis period, which makes it easier for the Heston model to match the option surface. In order to study this closer we divide the data set into two disjoint sets divided by the default of Lehman brothers on September 15, 2008. Table 5 reports the error measures computed on these two sets for the short maturity and far ITM call options on BTK and MSH. The table clearly shows that with the mentioned parameter reductions the contagion specifications are having difficulties pricing these options in the pre-crisis period. In the crisis period both contagion specifications perform better, but still slightly worse than the Heston model.

4. Pricing of multi-asset options

Pricing of European vanilla options can be done efficiently via Fourier transform methods (Carr and Madan, 1999; Lewis, 2001) using the characteristic function in (11), while knowledge of the extended transform in Eq. (17) allows for pricing of multi-asset options, such as spread and correlation options.

4.1. Correlation options

A correlation option is a two-factor version of a standard European call option. Take two assets S^1 and S^2. Then the correlation option has the payoff at maturity T

$$C\left(S_T^1, S_T^2; T, K_1, K_2\right) = \left(S_T^1 - K_1\right)^+ \cdot \left(S_T^2 - K_2\right)^+, \tag{39}$$

where $K_1, K_2 \geqslant 0$. Let $k_i = \log K_i$, then Dempster and Hong (2000) derive a pricing formula for the correlation option given by

$$\begin{aligned} C\left(S_t^1, S_t^2; t, T, K_1, K_2\right) &= e^{-\int_t^T r_s ds}\mathbb{E}\left[\left(S_T^1 - K_1\right)^+\left(S_T^2 - K_2\right)^+ | \mathcal{F}_t\right] \\ &= e^{-\int_t^T r_s ds}\frac{e^{-a_1 k_1 - a_2 k_2}}{4\pi^2}\int_{\mathbb{R}}\int_{\mathbb{R}} e^{-\mathrm{i}(u_1 k_1 + u_2 k_2)} \\ &\quad \times \Theta(u_1, u_2; t, T) du_1 du_2, \end{aligned} \tag{40}$$

where

$$\Theta(u_1, u_2; t, T) = \frac{\Phi(u_1 - (a_1+1)\mathrm{i}, u_2 - (a_2+1)\mathrm{i}; t, T)}{(a_1 + \mathrm{i}u_1)(a_1 + 1 + \mathrm{i}u_1)(a_2 + \mathrm{i}u_2)(a_2 + 1 + \mathrm{i}u_2)}, \tag{41}$$

with

$$\begin{aligned} \Phi(u_1, u_2; t, T) &= e^{\mathrm{i}u_1\int_0^T (r_s - q_s^1)ds} e^{\mathrm{i}u_2\int_0^T (r_s - q_s^2)ds}\psi_1^1(u_1, t, T)\psi_1^2(u_2, t, T) \\ &\quad \times \Psi(v, Y_t, t, T), \end{aligned} \tag{42}$$

$$v = [0 \quad 0 \quad u_1\mathrm{i} \quad u_2\mathrm{i}],$$

and $a_1, a_2 > 0$ are dampening factors used in the derivation of (40) to ensure the square-integrability of the option price. The Traffic

Table 5
The table reports the ARPE and the ARBAE (in parentheses) on the short maturity ($7 < T - t \leqslant 60$ days) and far ITM call options ($0.6 \leqslant K/S \leqslant 0.90$) on the BTK and MSH indexes. The pre-crisis period covers the days from April 9, 2007 to September 12, 2008 while the crisis period runs from September 15, 2008 to September 21, 2009. The ARPEs are reported in percentage, while the ARBAEs are reported in basis points.

Model	Heston	Negative exponential	Gaussian
BTK (i=1)			
Pre-crisis (658 obs.)	2.02 (0)	6.76 (33)	6.36 (28)
Crisis (1243 obs.)	2.04 (1)	2.85 (1)	2.79 (1)
MSH (i=2)			
Pre-crisis (1297 obs.)	3.18 (4)	6.20 (51)	5.86 (41)
Crisis (2164 obs.)	1.97 (0)	2.81 (1)	2.71 (1)

Light Option studied in Jørgensen (2007) and Kokholm (2009) is a particular case of a correlation option.

4.2. Spread options

Spread options are used in a wide area of applications in equity, commodities, and fixed income markets (see Carmona and Durrleman (2003) for a review). Consider a spread option on two assets S^1 and S^2 with payoff at maturity T and strike $K \geqslant 0$

$$S\left(S_T^1, S_T^2; T, K\right) = \left(S_T^1 - S_T^2 - K\right)^+. \tag{43}$$

Hurd and Zhou (2010) derive a pricing formula for spread options with $K = 1$ based on Fourier analysis of the payoff function

$$\begin{aligned} S\left(S_t^1, S_t^2; t, T, 1\right) &= e^{-\int_t^T r_s ds}\mathbb{E}\left[\left(S_T^1 - S_T^2 - 1\right)^+ | \mathcal{F}_t\right] \\ &= e^{-\int_t^T r_s ds}\frac{1}{4\pi^2}\int_{\mathbb{R}+i\vartheta_1}\int_{\mathbb{R}+i\vartheta_2}\Phi(u_1,u_2;t,T) \\ &\quad \times \widehat{P}(u_1,u_2)du_1du_2, \end{aligned} \tag{44}$$

where $\vartheta_2 > 0$ and $\vartheta_1 + \vartheta_2 < -1$,

$$\widehat{P}(u_1,u_2) = \frac{\Gamma(i(u_1+u_2)-1)\Gamma(-iu_2)}{\Gamma(iu_1+1)}, \tag{45}$$

and $\Gamma(z)$ is the complex gamma function defined by the integral

$$\Gamma(z) = \int_0^\infty e^{-t}t^{z-1}dt.$$

4.3. The impact of contagion on correlation, spread, and basket options

In this section we examine the impact of the cross-excitation parameters on the correlation, spread, and basket option prices for the two jump size specifications. The model parameters are set as those calibrated on September 21, 2009 and reported in Table 3. We will consider an example of the spread option payoff in (43) based on normalized index prices at 100, strike $K = 10$ and time to maturity $T = 1$. We take two different sets of underlyings: BTK-MSH and XBD-XNG. For the same sets of underlyings we compute prices of the correlation option with strikes equal to $K_1 = K_2 = 110$. Finally, we also consider a put basket option with payoff

$$B\left(S_T^1, S_T^2, S_T^3, S_T^4; T, K\right) = \left(K - \sum_{i=1}^4 S_T^i\right)^+, \tag{46}$$

where $K = 360$. The price is computed via simulation of 1 million sample paths generated using an Euler scheme.

As mentioned in Section 3.3, the cross-excitation parameters can be difficult to calibrate based on quotes on single-name options. Hence, we will consider the same three different scenarios for the cross-contagion parameters as in Section 2.5 to see how the contagion impact the multivariate option prices. In order to isolate the cross-excitation effect we will assume the instantaneous correlation between the indexes equal to zero. Besides the mentioned multi-name options we also price single-name OTM European put options on the indexes in order to compare the multi-name option price increases to increases on single-name options. Table 6 reports the resulting prices for the different scenarios together with the increase in the option price for scenarios (2) and (3) relative to the price in scenario (1). For both models we observe how the prices of all the options are increasing the higher the contagion and most dramatically for the correlation options. This is in accordance with intuition as higher contagion corresponds to higher volatility and higher correlation, where the latter is a key quantity in determining the price of correlation options. The out-of-the-money basket option price is also highly sensitive to the level of contagion as the probability for the contract to end in-the-money is sensitive to the level of contagion among the indexes. The contagion has a lower impact on the spread option price. On the one hand, will the increased contagion lead to higher volatility and thereby increase the price, but on the other hand will high contagion lead to higher correlation, which again will pull the price in the opposite direction, as the probability of realizing a big spread decreases.

5. Minimum variance hedging of derivatives in contagious markets

As the jump models described lead to incomplete markets, the European options cannot be replicated perfectly and there does not exist a unique hedge ratio. Hence, one has to choose a hedging criteria in order to derive a hedge portfolio. Here we will choose to minimize the expected variance of the hedging error. Besides leading to analytic tractability, this approach has the advantage of being linear, meaning that in order to hedge a portfolio of options on the same underlying it is sufficient to compute the hedge ratio for each individual option and then add them up (Tankov, 2011). Hedging of options in a contagion model of the type described has some interesting features studied in Section 5.1. When a shock occurs to one index this is reflected in changed dynamics of the other indexes, which has the consequence that the hedge ratio has to be updated for even simple European options on these other indexes. The number of shares $X_S(t)$ the hedger needs to hold at time t in order to minimize the variance of the call hedging error is solved in e.g. Arai (2005), Tankov (2011), and Cont et al. (2007),[4]

$$X_{S^i}^C(t) = \frac{Cov_t\left(dS_t^i, dC_t\right)}{Var\left(dS_t^i\right)} \tag{47}$$

$$= \frac{V_t^i\frac{\partial C_t}{\partial S_t^i} + \frac{V_t^i}{S_t^i}\rho_i\eta_i\frac{\partial C_t}{\partial V_t^i} + \frac{\lambda_t^i}{S_t^i}\mathbb{E}\left[\left(e^{\epsilon_n^i}-1\right)\left(C_t(S_t^i e^{\epsilon_n^i}, \lambda_t^i + \Delta\lambda_t^i) - C_t(S_t^i, \lambda_t^i)\right)|\mathcal{F}_t\right]}{V_t^i + V_{J_t^i}}, \tag{48}$$

where $C_t(S,\lambda)$ denotes the model call price in S, λ at time t and

$$V_{J_t^i} = \lambda_t^i\mathbb{E}\left[\left(e^{\epsilon_n^i}-1\right)^2\right]. \tag{49}$$

The resulting cash position equals

$$X_0^C(t) = C_t(S_t^i, \lambda_t) - X_{S^i}^C(t)S_t^i. \tag{50}$$

The hedge ratio for a put option on S^i can be found using the put-call parity

$$X_{S^i}^P(t) = X_{S^i}^C(t) - e^{-\int_t^T q_s^i ds}. \tag{51}$$

Except for $\mathbb{E}\left[\left(e^{\epsilon_n^i}-1\right)C_t(S_t^i e^{\epsilon_n^i}, \lambda_t^i + \Delta\lambda_t^i)|\mathcal{F}_t\right]$ all the terms in (47) are easily computable. Hence, with the help of the following proposition the hedge ratios can be computed.

Proposition 1. *(Jump and option covariance term) Let* $k_i = \log\left(\frac{S_i}{K}\right) + \int_t^T r_s - q_s^i ds$. *Then*

1. *For the intensity specification in (2) with the negative exponentially distributed jump sizes it holds that:*

[4] As in Bakshi et al. (1997). in order to simplify the analysis we assume that the underlying stock index is tradable. This is not a strict simplification as the correlation between the index and the index futures normally used for hedging is close to one.

$$\mathbb{E}\Big[\Big(e^{\epsilon_n^i}-1\Big)C_t(S_t^i e^{\epsilon_n^i},\lambda_t^i+\Delta\lambda_t^i)|\mathcal{F}_t\Big]=e^{-\int_t^T q_s^i ds}S_t^i\left(\frac{\gamma_i}{2+\gamma_i}-\frac{\gamma_i}{1+\gamma_i}\right)-\frac{\sqrt{S_t^i K}e^{-\frac{\int_t^T r_s+q_s^i ds}{2}}}{\pi}$$
$$\times\int_0^\infty\frac{\mathcal{R}\left\{e^{\mathrm{i}uk_i}\psi^i(u-\frac{\mathrm{i}}{2},t,T)\left(\frac{\gamma_i}{\frac{3}{2}+\mathrm{i}u+\gamma_i+\sum_{j=1}^M\delta_{j,i}b_j(t)}-\frac{\gamma_i}{\frac{1}{2}+\mathrm{i}u+\gamma_i+\sum_{j=1}^M\delta_{j,i}b_j(t)}\right)\right\}}{u^2+\frac{1}{4}}du. \tag{52}$$

2. *For the intensity specification (3) with the normally distributed jump sizes it holds that:*

$$\mathbb{E}\Big[\Big(e^{\epsilon_n^i}-1\Big)C_t(S_t^i e^{\epsilon_n^i},\lambda_t^i+\Delta\lambda_t^i)|\mathcal{F}_t\Big]=e^{-\int_t^T q_s^i ds}S_t^i\left(e^{2\beta_i+2\sigma_i^2}-e^{\beta_i+\frac{\sigma_i^2}{2}}\right)-\frac{\sqrt{S_t^i K}e^{-\frac{\int_t^T r_s+q_s^i ds}{2}}}{\pi}$$
$$\times\int_0^\infty\frac{\mathcal{R}\left\{e^{\mathrm{i}uk_i}\psi^i(u-\frac{\mathrm{i}}{2},t,T)e^{\sum_{j=1}^M\delta_{j,i}b_j(t)}\left(e^{(\frac{3}{2}+\mathrm{i}u)\beta_i+(\frac{9}{8}-\frac{1}{2}u^2+\frac{3}{2}\mathrm{i}u)\sigma_i^2}-e^{(\frac{1}{2}+\mathrm{i}u)\beta_i+(\frac{1}{8}-\frac{1}{2}u^2+\frac{1}{2}\mathrm{i}u)\sigma_i^2}\right)\right\}}{u^2+\frac{1}{4}}du. \tag{53}$$

Proof. The price of a call option can be related to the underlying via (33). Both the results then follow by integration on the expectations and by the use of Tonelli's Theorem. □

Say that index i does not trade liquidly and you want to hedge a position in an option on asset i. In this case one can hedge the option by investing in asset j. An application of Itô's Lemma reveals that the investment in index j for hedging a call option on index i equals

$$X_{S^j}^{C^i}(t)=\frac{\frac{S_t^i}{S_t^j}\sqrt{V_t^jV_t^i}\frac{\partial C^i}{\partial S^i}\rho_{i,j}+\frac{\sqrt{V_t^jV_t^i}}{S_t^j}\eta^i\rho_{j,v^i}\frac{\partial C^i}{\partial V_t^i}+\frac{\lambda_t^j}{S_t^j}\mathbb{E}\Big[\Big(e^{\epsilon_n^j}-1\Big)\Big(C_t(S_t^i,\lambda_t^i+\Delta\lambda_t^i)-C_t(S_t^i,\lambda_t^i)\Big)|\mathcal{F}_t\Big]}{V_t^j+V_{J_t^j}}, \tag{54}$$

where $dW_t^j dW_t^i=\rho_{i,j}dt$ and $dW_t^j dZ_t^i=\rho_{j,v^i}dt$.

The following corollary details the analytic form of $\mathbb{E}\Big[\Big(e^{\epsilon_n^j}-1\Big)C_t(S_t^i,\lambda_t^i+\Delta\lambda_t^i)|\mathcal{F}_t\Big]$.

Corollary 1. *(Cross jump and option covariance term)*

1. *For the intensity specification in (2) with the negative exponentially distributed jump sizes it holds that:*

Table 6
Spread, correlation, basket and put option prices in the three scenarios in the three different model specifications. The initial index prices are normalized at 100 and the time to maturity equals 1 year for all the options. For the spread options the strike is $K=10$, for the correlation options the strikes are identical $K_1=K_2=110$, for the basket option $K=360$, and the put options all have $K=90$. The option price increase relative to the zero cross-excitation price is reported in percentage (in parentheses).

Option type:	Spread		Correlation		Basket	Put			
Indexes:	BTK-MSH	XBD-XNG	BTK-MSH	XBD-XNG	All four	BTK	MSH	XBD	XNG
Heston	11.8	14.8	46.9	86.6	10.2	7.4	7.3	8.6	9.6
Negative exponential jumps									
No cross-excitation	9.9	13.1	31.3	67.4	8.2	6.4	6.1	7.4	8.4
Base case	11.2	14.5	41.0	80.4	10.4	7.3	7.2	8.5	9.5
	(13.5)	(10.8)	(31.0)	(19.4)	(25.5)	(15.0)	(18.9)	(15.0)	(12.9)
Heavy cross-excitation	14.4	17.6	72.3	114.7	16.2	9.7	9.9	11.1	12.1
	(45.1)	(34.7)	(130.9)	(70.4)	(96.3)	(52.0)	(63.0)	(50.4)	(44.7)
Gaussian jumps									
No cross-excitation	9.9	13.1	31.3	66.7	8.3	6.6	5.8	7.3	8.5
Base case	11.3	14.7	40.5	83.3	10.6	7.4	7.3	8.6	9.6
	(14.4)	(12.2)	(29.2)	(24.9)	(27.9)	(10.9)	(26.0)	(17.4)	(13.7)
Heavy cross-excitation	14.0	17.6	66.2	123.2	15.9	9.1	10.0	11.1	12.0
	(42.2)	(34.9)	(111.3)	(84.7)	(92.4)	(37.4)	(73.1)	(51.9)	(41.6)

$$\mathbb{E}\left[\left(e^{\epsilon_n^j}-1\right)C_t(S_t^i,\lambda_t^i+\Delta\lambda_t^i)|\mathcal{F}_t\right]$$
$$=e^{-\int_t^T q_s^i ds}S_t^i\left(\frac{\gamma_j}{1+\gamma_j}-1\right)-\frac{\sqrt{S_t^iK}e^{-\frac{\int_t^T r_s+q_s^i ds}{2}}}{\pi}$$
$$\times\int_0^\infty\frac{\mathcal{R}\left\{e^{\mathrm{i}uk_i}\psi^i(u-\frac{\mathrm{i}}{2},t,T)\left(\frac{\gamma_j}{1+\gamma_j+\sum_{i=1}^M\delta_{ij}b_i(t)}-\frac{\gamma_j}{\gamma_j+\sum_{i=1}^M\delta_{ij}b_i(t)}\right)\right\}}{u^2+\frac{1}{4}}du. \tag{55}$$

2. *For the intensity specification (3) with the normally distributed jump sizes it holds that:*

$$\mathbb{E}\left[\left(e^{\epsilon_n^j}-1\right)C_t(S_t^i,\lambda_t^i+\Delta\lambda_t^i)|\mathcal{F}_t\right]$$
$$=e^{-\int_t^T q_s^i ds}S_t^i\left(e^{\beta_j+\frac{\sigma_j^2}{2}}-1\right)-\frac{\sqrt{S_t^iK}e^{-\frac{\int_t^T r_s+q_s^i ds}{2}}}{\pi}$$
$$\times\int_0^\infty\frac{\mathcal{R}\left\{e^{\mathrm{i}uk_i}\psi^i(u-\frac{\mathrm{i}}{2},t,T)e^{\sum_{i=1}^M\delta_{ij}b_i(t)}\left(e^{\beta_j+\frac{\sigma_j^2}{2}}-1\right)\right\}}{u^2+\frac{1}{4}}du. \tag{56}$$

Proof. The same as the proof of Proposition 1. □

5.1. Impact of contagious jumps on prices and hedge ratios

Since the dynamics of an index i and the price of an option on index i will change if a jump occurs in index $j\neq i$, the hedge ratio will have to be updated although the value of index i has not changed. In this Section we perform a numerical study of the impact of a jump in another asset on the hedge ratios in (47) and on option prices. Again we consider the three contagion scenarios detailed in Section 2.5 and compute the hedge ratio and the price of an option on the BTK index. We compare this to the value of both quantities conditioned on a jump in the XNG index.[5] Table 7 reports the result for an OTM call option with maturity $T=\frac{1}{2}$ and with strike equal to $K=1.1$ and $S_0^1=1$.

As expected we see that in the scenario with no cross-excitation, a jump in XNG does not affect either the price or the hedge ratio. In the base scenario, the jump in XNG has a significant impact on the option price resulting in an increase of more than 135%, and more than 220% in the highly contagious regime. This small example highlights what can be the potential drawbacks of ignoring contagion effects. Namely, that it can lead to an underestimation of the risks associated with options trading. Interestingly, we observe how the hedge ratio before the jump does not depend on the scenario as the local dynamics of the assets depend on the instantaneous intensity of jumps and the distribution of the jump sizes, but not on the cross-contagion parameters. However, the change in the hedge ratio does depend on the scenario as the post-jump level of the intensity depends on the cross-excitation parameters.

5.2. Hedging performances of the models

In this section we study the hedging performances of the model specifications. We take the time series of options data on the four markets from April 9, 2007 to September 21, 2009 and study the historical hedging performance of the two proposed mutually self-exciting jump specifications and include the Heston model as benchmark. On each day the models are re-calibrated as described in Section 3.5. Then, the hedge ratios in (47) and (51) are computed with the calibrated model on each day in the period. With the computed hedge ratios the hedging errors on the call options on each day are computed as

$$\varepsilon^C(t)=C_t(S_t^i,\lambda_t)-X_{S^i}^C(t-1)S_t^i-X_0^C(t-1)e^{r_{t-1}\Delta t} \tag{57}$$

The relative hedging error (RHE) is defined as the absolute error relative to the observed option quote on the particular day. In order to keep the error due to the discrete hedging in time limited, we only record the hedging error if there is an option quote on the previous business day. Again, we compute the errors for the same categories of moneyness and maturity as in the pricing analysis.

On each index and for each model, Table 8 reports the risk measures Average Relative Hedging Error (ARHE) for the different option categories across calendar dates.

For all the indexes the Heston model is the winner followed by the negative exponential jump specification, which is performing slightly better than the Gaussian jump specification in most of the option categories.

The contagion specifications perform worse than the Heston model since the dynamics are estimated under a pricing measure, while the hedging errors are computed based on the "physical" dynamics of the indexes. Especially in markets where the risk aversion is high and there is a heavy risk premium to negative jumps, models exhibiting jumps will be punished more under the "physical" measure than models with continuous paths (see Cont et al., 2007). Hence, it would be more natural to perform the hedging under the statistical measure, but in this case one would have to estimate the dynamics from historical observations on the stock returns over an extended period. On the contrary, hedging of options is done from day to day on a local time scale. It is out of the scope of this paper to contribute to this discussion and we refer the reader to Tankov (2011) for a discussion of both approaches. Our hedging results are also in line with the study in Bakshi et al. (1997), where the authors find that for hedging options on S&P 500 stochastic volatility models perform better than jump models, when the models are estimated under the risk-neutral measure. In a more recent study, Kaeck (2013) finds that taking jumps into account does in fact improve hedging performances, when the underlying asset dynamics are estimated based on both options markets and historical observations on the underlying return dynamics.

Table 7
The sensitivity of call option prices and hedge ratios to contagious jumps in the two contagion specifications. The call option has maturity $T=\frac{1}{2}$, strike $K=1.1$, and the index BTK as underlying security with normalized time-0 value equal to $S_0^1=1$. For the three contagion scenarios the price and the hedge ratio are computed before and after a jump in the value of the XNG index.

Scenario	No cross-excitation		Base Scenario		Heavy cross-excitation	
Jump in the XNG index	No	Yes	No	Yes	No	Yes
Negative exponential jumps						
Call option price	0.031	0.031	0.034	0.080	0.036	0.116
Hedge ratio	0.191	0.191	0.191	0.174	0.191	0.162
Gaussian jumps						
Call option price	0.032	0.032	0.034	0.081	0.035	0.119
Hedge ratio	0.182	0.182	0.182	0.165	0.182	0.153

6. Conclusion

We model contagion between markets by including mutually exciting jump processes in the dynamics of the indexes'

[5] In the negative exponential jump specification we condition on a jump in the log of the XNG index equal to the mean jump size $\frac{1}{\gamma_4}$.

Table 8
The table reports the average relative hedging errors for different levels of moneyness and maturity across the observation dates for the four indexes and the three models. All the reported numbers are in percentage.

			Days to expiration			
Index	Moneyness K/S	Model	$\leqslant 60$	60–180	>180	All
BTK	$\leqslant$0.90	Heston	0.73	0.87	0.83	0.83
		Neg. exp.	1.56	1.53	1.19	1.44
		Gaussian	1.41	1.8	1.89	1.76
	0.9–1.0	Heston	2.57	2.59	1.90	2.45
		Neg. exp.	4.22	3.51	2.35	3.58
		Gaussian	3.89	4.08	3.48	3.90
	1.0–1.1	Heston	12.09	7.91	3.79	8.58
		Neg. exp.	13.59	9.18	4.55	9.83
		Gaussian	13.11	10.99	6.53	10.85
	>1.1	Heston	19.57	17.97	9.92	14.74
		Neg. exp.	24.79	23.71	16.49	20.79
		Gaussian	19.68	30.17	20.47	25.31
	All	Heston	6.59	6.66	4.54	6.09
		Neg. exp.	8.26	8.61	6.99	8.10
		Gaussian	7.63	10.65	9.08	9.44
MSH	$\leqslant$0.90	Heston	0.74	0.81	0.75	0.78
		Neg. exp.	1.62	1.45	1.22	1.40
		Gaussian	1.35	1.58	1.75	1.60
	0.9–1.0	Heston	2.96	2.64	1.89	2.58
		Neg. exp.	4.29	3.66	2.93	3.63
		Gaussian	3.84	4.12	3.50	3.89
	1.0–1.1	Heston	13.87	7.21	3.43	8.51
		Neg. exp.	15.52	8.78	4.60	10.01
		Gaussian	15.18	10.21	6.47	10.93
	>1.1	Heston	19.43	15.80	7.01	12.78
		Neg. exp.	27.31	24.77	13.17	20.56
		Gaussian	22.90	24.33	13.73	20.10
	All	Heston	7.85	6.03	3.25	5.65
		Neg. exp.	9.80	8.80	5.48	8.08
		Gaussian	9.03	9.19	6.36	8.34
XBD	$\leqslant$0.90	Heston	1.34	1.36	1.27	1.33
		Neg. exp.	2.1	1.82	1.57	1.80
		Gaussian	1.65	1.85	1.81	1.80
	0.9–1.0	Heston	3.17	3.11	2.55	3.03
		Neg. exp.	4.31	3.89	3.7	3.89
		Gaussian	3.56	3.91	3.46	3.68
	1.0–1.1	Heston	9.11	6.41	4.03	6.94
		Neg. exp.	10.43	7.57	4.85	8.09
		Gaussian	9.0	7.68	5.6	7.76
	>1.1	Heston	16.54	11.62	7.52	10.82
		Neg. exp.	21.81	14.64	10.28	14.07
		Gaussian	17.24	15.23	12.33	14.46
	All	Heston	6.53	5.67	4.19	5.49
		Neg. exp.	8.26	8.95	5.51	6.96
		Gaussian	6.81	7.28	6.52	6.95
XNG	$\leqslant$0.90	Heston	0.73	0.85	0.82	0.82
		Neg. exp.	1.35	1.31	1.1	1.26
		Gaussian	1.11	1.49	1.63	1.46
	0.9–1.0	Heston	2.42	2.44	1.85	2.33
		Neg. exp.	3.34	2.98	2.24	2.98
		Gaussian	3.05	3.49	3.0	3.23
	1.0–1.1	Heston	8.85	5.68	3.3	6.38
		Neg. exp.	9.18	6.12	3.87	6.8
		Gaussian	8.99	7.33	5.01	7.49
	>1.1	Heston	15.47	11.31	6.06	10.22
		Neg. exp.	16.14	14.23	9.72	13.09
		Gaussian	15.37	15.65	9.89	13.75
	All	Heston	5.88	4.94	3.08	4.73
		Neg. exp.	6.55	6.04	4.47	5.79
		Gaussian	6.21	6.83	6.2	6.22

log-returns, so that a jump in one market increases the intensities of more jumps in the same market and in other markets. Between jumps, the intensities revert to their long-run means. On top of this, we add a stochastic volatility component to the dynamics in order to introduce more flexibility in the log-return process enabling a fit to individual option implied volatility surfaces. Due to the affine model specification, the joint characteristic function of the log-returns is known analytically, and for two specifications we detail how the model can be calibrated efficiently to option prices using Fourier transform methods. In total, we calibrate the specifications to options data on the BTK, MSH, XBD, and the XNG indexes. In order to reduce computational time, the calibration is performed in two steps. First, the parameters of the mutually exciting processes are calibrated for the indexes simultaneously to data for the shortest maturity options. Second, the stochastic volatility dynamics are calibrated to the whole option surface on each index independently. We show that the model is able to simultaneously fit option volatility surfaces of four indexes over an extended period of time. Moreover, we illustrate how the level of contagion has a heavy positive impact on correlation and basket option prices. For the spread option the impact on the price is positive but less pronounced since the increased correlation pulls the price down. We derive hedge ratios on European put and call options and perform a numerical experiment highlighting the impact of contagious jumps on option prices and hedge ratios. Finally, we perform a historical hedging experiment with the calibrated model specifications.

Acknowledgments

This paper was presented at the 22nd Annual Derivatives Securities and Risk Management Conference, the 7th Bachelier Finance Society World Congress, Research in Options 2012, the Finance and Stochastics Seminar Series – Imperial College, and the Accounting and Finance Seminar Series – University of Southern Denmark. Thanks to the Danish Council for Independent Research | Social Sciences for financial support. I wish to thank two anonymous referees, Peter Carr, Rama Cont, Dilip Madan, Elisa Nicolato, David Skovmand and David Sloth Pedersen for providing valuable comments. Wharton Research Data Services (WRDS) was used in preparing this manuscript. This service and the data available thereon constitute valuable intellectual property and trade secrets of WRDS and/or its third-party suppliers.

Appendix A. Existence and uniqueness

Following the notation of Kallsen (2006) the process defined as

$$\widetilde{Y}_t = \left[\lambda_t^1 \quad \dots \quad \lambda_t^m \quad J_t^1 \quad \dots \quad J_t^m\right]^\top$$

is affine with differential characteristics

$$\tilde{\beta}(y) = \tilde{\beta}_0 + \sum_{j=1}^{2m} y^j \tilde{\beta}_j \tag{58}$$

$$\tilde{\gamma}(y) = 0 \tag{59}$$

$$\tilde{\varphi}(y, G) = \sum_{j=1}^{2m} y^j \tilde{\varphi}_j(G), \quad G \in \mathcal{B}^{2m} \tag{60}$$

with the Lévy-Kintchine triplets on $\mathbb{R}^{2m}$ given as

$$\tilde{\beta}_0 = \left[\alpha_1\bar{\lambda}_1 \quad \dots \quad \alpha_m\bar{\lambda}_m \quad \underline{\mathbf{0}}\right]^\top, \quad \tilde{\beta}_j = \left[-\alpha_j e_j \quad \underline{\mathbf{0}}\right]^\top$$

$$\tilde{\varphi}_j(G) = \begin{cases} \int_{\mathbb{R}^{2m}} \mathbb{1}_G\left(\zeta^j \underline{z}\right) d\underline{F}^j(\underline{z}) & \text{for } j = 1, \dots, m \\ 0 & \text{for } j = m+1, \dots, 2m. \end{cases} \qquad \underline{z} \in \mathbb{R}^{2m},$$

where $\underline{\mathbf{0}}$ denotes a $1 \times m$-dimensioned vector of zeros and e_i the unit vector, a $1 \times m$ vector with 1 at the i'th entry and zeros at all other entries. $\underline{F}^j$ is the fixed jump distribution of the pure jump process defined in either (22) or in (24) depending on the specific intensity specification. By Theorem 3.2 in Kallsen (2006) the process $\widetilde{Y}$ exists and is uniquely characterized by its conditional characteristic function if

$$1: \quad \tilde{\beta}_0^k = \alpha_k \bar{\lambda}_k \geqslant 0 \quad \text{for all } k = 1, \ldots, m \tag{61}$$

$$2: \quad \tilde{\varphi}_j\left(\left(\mathbb{R}_+^m \times \mathbb{R}^m\right)^C\right) = 0 \quad \text{for all } j = 1, \ldots, m \tag{62}$$

$$3: \quad \begin{cases} \int \delta_{k,j} z dF^j(z) < \infty & \text{for all } k,j = 1, \ldots, m \quad \text{(Neg. exp. jumps)} \\ \delta_{k,j} < \infty & \text{for all } k,j = 1, \ldots, m \quad \text{(Gaussian jumps)}. \end{cases} \tag{63}$$

The condition in (61) clearly holds in both specifications as $\alpha_i, \bar{\lambda}_i > 0$ for all $i = 1, \ldots, m$. The non-negativity conditions of the jumps in the intensities (62) are also fulfilled, in the Gaussian jump case when $\delta_{i,j} > 0$, and in the negative exponential jump case when $\delta_{i,j} < 0$ and $\gamma_i > 0$ for all $i,j = 1, \ldots, m$. The final condition (63) clearly also holds as long as the mean of the jump sizes and the $\delta_{k,j}$ are finite.

Appendix B. Martingality of the price dynamics

Define

$$Y_t = \left[\lambda_t^1 \quad \ldots \quad \lambda_t^m \quad -\xi_1 \int_0^t \lambda_s^1 ds + J_t^1 \quad \ldots \quad -\xi_m \int_0^t \lambda_s^m ds + J_t^m \right]^\top.$$

If for all $t \geqslant 0$ it holds that

$$1: \quad \int e^z dF^j(z) < \infty, \quad \text{for } j = 1, \ldots, m \tag{64}$$

$$2: \quad -\xi_j + \int (e^z - 1) dF^j(z) = 0, \quad \text{for } j = 1, \ldots, m \tag{65}$$

$$3: \quad \begin{cases} \int \delta_{k,j} z e^z dF^j(z) < \infty & \text{for all } k,j = 1, \ldots, m \quad \text{(Neg. exp. jumps)} \\ \int \delta_{k,j} e^z dF^j(z) < \infty & \text{for all } k,j = 1, \ldots, m \quad \text{(Gaussian jumps)}. \end{cases}, \tag{66}$$

then the processes defined by $e^{Y_t^i}, i = m+1, \ldots, 2m$ are martingales (Kallsen and Muhle-Karbe, 2010), and hence, also the processes with dynamics (4) being the product of two independent exponential martingales. The condition (64) is clearly fulfilled in the two proposed jump specifications. The condition (65) is satisfied by construction. The final condition is satisfied in the Gaussian jump specification due to the jumps being normally distributed. One can realize that it is also fulfilled for the negative exponential jump specification as $e^z < 1$ for $z < 0$.

References

Aït-Sahalia, Y., Cacho-Diaz, J., Laeven, R.J., 2015. Modeling financial contagion using mutually exciting jump processes. Journal of Financial Economics 117 (3), 585–606.

Aït-Sahalia, Y., Hurd, T.R., 2015. Portfolio choice in markets with contagion. Journal of Financial Econometrics 14 (1), 1–28.

Aıt-Sahalia, Y., Laeven, R.J., Pelizzon, L., 2014. Mutual excitation in Eurozone sovereign CDS. Journal of Econometrics 183 (2), 151–167.

Andersen, L., Andreasen, J., 2002. Volatile volatilities. RISK Magazine 15 (12), 163–163.

Arai, T., 2005. An extension of mean-variance hedging to the discontinuous case. Finance and Stochastics 9 (1), 129–139.

Bakshi, G., Cao, C., Chen, Z., 1997. Empirical performance of alternative option pricing models. Journal of Finance 52 (5), 2003–2049.

Bowsher, C.G., 2007. Modelling security market events in continuous time: intensity based, multivariate point process models. Journal of Econometrics 141 (2), 876–912.

Carmona, R., Durrleman, V., 2003. Pricing and hedging spread options. Siam Review 45 (4), 627–685.

Carr, P., Madan, D., 1999. Option valuation using the fast Fourier transform. Journal of Computational Finance 2 (4), 61–73.

Carr, P., Madan, D.B., 2005. A note on sufficient conditions for no arbitrage. Finance Research Letters 2 (3), 125–130.

Cont, R., Tankov, P., 2004. Nonparametric calibration of jump-diffusion option pricing models. Journal of Computational Finance 7 (3), 1–49.

Cont, R., Tankov, P., Voltchkova, E., 2007. Hedging with options in models with jumps. In: Stochastic Analysis and Applications, pp. 197–217.

Cousot, L., 2007. Conditions on option prices for absence of arbitrage and exact calibration. Journal of Banking and Finance 31 (11), 3377–3397.

Dempster, M., Hong, S., 2000. Spread option valuation and the fast Fourier transform. Technical report. The Judge Institute of Management Studies, University of Cambridge.

Duffie, D., Filipović, D., Schachermayer, W., 2003. Affine processes and applications in finance. Annals of Applied Probability 13 (3), 984–1053.

Duffie, D., Pan, J., Singleton, K., 2000. Transform analysis and asset pricing for affine jump-diffusions. Econometrica 68 (6), 1343–1376.

Errais, E., Giesecke, K., Goldberg, L., 2010. Affine point processes and portfolio credit risk. SIAM Journal on Financial Mathematics 1 (1), 642–665.

Fry-McKibbin, R., Martin, V.L., Tang, C., 2014. Financial contagion and asset pricing. Journal of Banking and Finance 47, 296–308.

Gatheral, J., 2006. The Volatility Surface: A Practitioner's Guide. Wiley.

Gouriéroux, C., Jasiak, J., Sufana, R., 2009. The Wishart autoregressive process of multivariate stochastic volatility. Journal of Econometrics 150 (2), 167–181.

Hawkes, A., 1971. Spectra of some self-exciting and mutually exciting point processes. Biometrika 58 (1), 83–90.

Heston, S., 1993. A closed-form solution for options with stochastic volatility with applications to bond and currency options. Review of Financial Studies 6 (2), 327.

Hurd, T., Zhou, Z., 2010. A Fourier transform method for spread option pricing. Siam Journal on Financial Mathematics 1 (1), 142–157.

Jrgensen, P., 2007. Traffic light options. Journal of Banking and Finance 31 (12), 3698–3719.

Jrgensen, P., Nrholm, H., Skovmand, D., 2011. Overpricing and hidden costs of structured bonds for retail investors: evidence from the Danish market for principal protected notes. Working paper.

Kaeck, A., 2013. Hedging surprises, jumps, and model misspecification: a risk management perspective on hedging S&P 500 options. Review of Finance 17 (4), 1535–1569.

Kallsen, J., 2006. A didactic note on affine stochastic volatility models. From Stochastic Calculus to Mathematical Finance. Springer, pp. 343–368.

Kallsen, J., Muhle-Karbe, J., 2010. Exponentially affine martingales, affine measure changes and exponential moments of affine processes. Stochastic Processes and their Applications 120 (2), 163–181.

Karabash, D., 2012. On stability of Hawkes process. Working paper.

Kokholm, T., 2009. Pricing of traffic light options and other hybrid products. International Journal of Theoretical and Applied Finance 12 (05), 687–707.

Leoni, P. and Schoutens, W., 2008. Multivariate smiling. Wilmott Magazine, March.

Lewis, A., 2001. A simple option formula for general jump-diffusion and other exponential Lévy processes. Envision Financial Systems and OptionCity.net.

Luciano, E., Semeraro, P., 2010. Multivariate time changes for Lévy asset models: characterization and calibration. Journal of Computational and Applied Mathematics 233 (8), 1937–1953.

Madan, D.B., 2011. Joint risk-neutral laws and hedging. IIE Transactions 43 (12), 840–850.

Schoutens, W., Simons, E., Tistaert, J., 2004. A perfect calibration! now what? Wilmott Magazine, March.

Shephard, N.G., 1991. From characteristic function to distribution function: a simple framework for the theory. Econometric Theory 7 (4), 519–529.

Tankov, P., 2011. Pricing and hedging in exponential Lévy models: review of recent results. Paris-Princeton Lectures on Mathematical Finance 2010, 319–359.

Wallmeier, M., Diethelm, M., 2012. Multivariate downside risk: normal versus variance gamma. Journal of Futures Markets 32 (5), 431–458.